

Detecting and tracking of airborne volcanic ash with the WSR-88Ds

Valery Melnikov^{*#}, Richard Murnan⁺, and Donald Burgess^{*#}

^{*}Cooperative Institute for Mesoscale Meteorological Studies, the University of Oklahoma

⁺Radar Operations Center, the National Weather Service

[#]NOAA/OAR National Severe Storms Laboratory

Report on task 8 of 2016 ROC MOU

This work was funded by the NWS Radar Operations Center

September 2016

Contents

Abstract	3
1. Introduction.....	4
2. Observations of volcanic ash with C- and X-band radars outside the USA	6
2.1. Eruption of volcano Hekla, Iceland in February 2000	8
2.2. Eruption of Grímsvötn, Iceland on 2 November 2004	10
2.3. Eruption of Eyjafjöll, Iceland in April 2010	11
2.4. Eruption of Etna, Italy in April 2011	13
2.5. Eruption of Grímsvötn, Iceland in May 2011	15
2.6. Eruption of Mt Kelud, Indonesia in February 2014	16
2.7. Eruption of Calbuco, Chili in April 2015	17
2.8. Characteristics of radars used to observe airborne volcanic ash	19
3. Observations of wild fire ash with the dual-pol WSR-88D	20
4. Observations of volcanic ash with weather radars in the USA.....	24
4.1. Eruption of St. Helens in March 1982.....	29
4.2. Eruption of Mt Spurr volcano in Alaska in August - September 1992.....	30
4.3. Eruption of Mt Augustine in January 2006.....	31
4.4. Eruption of Mt Redoubt in 2009	33
4.5. Eruption of Anatahan in April 2005	35
4.6. Eruption of Pavlof volcano in March 2016	35
4.7. Comparison of radar sensitivities	38
4.8. Dual polarization properties of volcanic ash.....	39
5. Techniques to increase detectability of radar echoes.....	42
5.1. Spectral processing to enhance detectability.....	42
5.2. Coherent summation	43
5.3. De-speckling of radar fields.....	45
6. Summary	46
7. Recommended VCPs for radar observations of volcanic ash	48
References	51

Abstract

Of the 169 geologically active volcanoes in the USA, 54 volcanoes have the USGS threat levels of "high" or worse. Seven from the ten most dangerous volcanoes in the US are located in the highly populated states of Washington, Oregon, and California. Several WSR-88Ds are located in the volcanic areas and can be used to detect explosive eruptions, estimate the amount of ash erupted, and track the volcanic plumes. These radar capabilities can be used to estimate a hazard for the general public and aviation. The estimated erupted volcanic mass could be used by the atmospheric transport models to predict propagation of ash plumes at large distances from volcanoes.

The majority of radar observations of airborne volcanic ash have been conducted with C-band weather radars although there are a few reports on using X- and S-band systems. Comparisons of sensitivity of radars which have been used to observe volcanic ash with that of the WSR-88D show that the latter has a better sensitivity to detect the ash. The WSR-88Ds are capable of detecting explosive eruptions at distances at least 320 km. Polarization properties of the ash are discussed and compared with the ones of wild fire ash. Some signal processing techniques to enhance detectability of radar echoes are considered. Recommendations of radar settings to observe airborne volcanic ash with the WSR-88Ds are made.

1. Introduction

Airborne volcanic ash is a hazard to aviation and is a hazardous substance for human health (e.g., Cadle et al. 1979). Wet ash conducts electricity, so it can cause the failure of various electronic devices (e.g., Rose et al. 1995a). Small ash particles injected into the upper troposphere and stratosphere can reside there for years and affect global weather and climate (Graf et al. 2007). Global aviation operates around the world including regions with active volcanoes such as Indonesia, Japan, Central and South America, and Alaska. Volcanic ash is especially dangerous for modern aviation (Casadevall 1994, Rose et al. 1995a). Small ash particles can go through the air filters and cause damage to the engines and electric equipment of airplanes. The ash from the Eyjafjöll Icelandic volcano in 2010 caused cancellations and delays of enormous numbers of flights over Europe for more than a month (Zehner 2010). Icelandic volcanic activity poses a major hazard to airplane traffic in the North Atlantic area. More than 250 jet airplanes use this area daily. Thus monitoring volcanic eruption in Iceland is very important for aviation. The monitoring of volcanic activity in Alaska is important for aviation as well. Avoidance of volcanic ash is the only procedure which guarantees flight safety (Cantor 1998). Volcanic plumes with ash concentration as low as 0.2 g m^{-3} can be produced in extremely weak eruptions of duration less than 1 min. Therefore ash clouds, regardless of eruption magnitude, are a serious hazard for aviation (Harris and Rose 1983). Because of the significance of the hazards posed by airborne volcanic ash, its timely detection and tracking in the atmosphere is very important.

The fragments of magma and parts of the volcanic system that are thrown up into the atmosphere during eruptions is called tephra. Together with volcanic gases they form a volcanic plume. Volcanic ash is a part of tephra with particles of sizes smaller than 2 mm. Such small particles can reside in the atmosphere for days, months, and even years (Graf et al. 2007, Marzano 2012b). Radar data can be used to estimate concentration and the mean size of ash particles (e.g., Marzano et. al. 2013a, Mereu et al. 2015).

Volcanic ash in the atmosphere can be detected and tracked with radars operating at various wavelengths. The S-band WSR-88D radars have been designed to monitor severe weather and to measure precipitation. Sensitivity of the radar is extremely high and allows observations of smoke plumes and even clear air. Radar observations show that volcanic eruptions can be detected at distances longer than 300 km (section 4.5) and propagation of smoke plumes can be monitored with the WSR-88D radars.

Some volcanic eruptions have been observed with the WSR-88Ds. Radar detectability of volcanic particles depends on their sizes, dielectric permittivity, number concentration, and the distance to radar. The parameters of volcanic particles in the atmosphere depend on volcano type and the intensity of eruptions. The majority of radar observations of volcanic ashes have been conducted with C-band weather radars having the wavelengths about 5.6 cm (e.g., Rose et al. 1995a,b, Sawada 2004, Marzano et al. 2006, 2010, Vulpiani et al. 2011, Wardojo 2015, Vidal et al. 2015). A few observations at X frequency band (the wavelength of 3.2 cm) have also been documented by Maki et al (2001) and Marzano et al. (2012b). Speirs and Robertson (2011) observed airborne volcanic ash with mm-wavelength radars.

Radar monitoring of volcano eruptions allows

- determining the time and duration of eruption, which is very important for the models which calculate ash transport in the atmosphere,
- estimating the ash mass erupted,
- monitoring the transport of ashes in the atmosphere,
- estimating hazards for aviation and the general public.

The goals of this report are as follows.

- Observations of volcanic ash with the WSR-88D are limited. So a review of observations of the ash with various weather radars is provided in section 2. Using the parameters of radars with documented observations of the ash, sensitivity of these radars should be compared with sensitivity of the WSR-88D. The distance, at which detection of ash with the WSR-88D is feasible, should be estimated.
- History of dual-polarization radars is not so long yet, so dual-pol observations of volcanic ash are not comprehensive. The dual-polarization characteristics of ash should be analyzed to make recommendations on distinguishing an ash plume echo from precipitation and clear air echoes. Wild fire ash has been observed with the polarimetric WSR-88D. The properties of smoke ash should be compared with ones measured in volcanic ash (section 4.8).
- An analysis of radar observations of volcanic ash in the USA is provided in section 4, where the dual pol properties of the ash are also discussed.

- To observe volcanic ash at long distances, possible enhancements of detectability of weak echoes should be analyzed. Such enhancements can be achieved with special signal processing discussed in section 5.
- Some recommendations for dual-pol radar observations of airborne ash are presented in section 7.

2. Observations of volcanic ash with C- and X-band radars outside the USA

Volcanic ash clouds contain tephra particles of different sizes and are distributed targets for radars. The mean received power \bar{P}_r from distributed scatterers in the radar resolution volume can be written as (Doviak and Zrnic 2006, section 4.4.1),

$$\bar{P}_r = \frac{P_t g^2 c \tau \pi \theta_1^2 \lambda^2 \eta}{16 \ln 2 (4\pi)^3 R^2 l^2}, \quad (2.1)$$

where P_t , being the transmit power, g antenna gain, c speed of light, τ pulse duration, θ_1 3-dB beamwidth, λ wavelength, l signal losses, R distance to the resolution volume, and η reflectivity. The latter variable is connected to reflectivity factor Z as,

$$Z = 10 \log \left(\frac{\lambda^4}{\pi^5} \left| \frac{\varepsilon - 1}{\varepsilon + 2} \right|^2 \eta \right) \quad (\text{dBZ}), \quad (2.2)$$

where ε is dielectric permittivity of scatterers. Reflectivity η is the backscatter cross section of scatterers in unit volume ΔV (Doviak and Zrnic 2006, section 4.4.5):

$$Z = 10 \log \left(\frac{1}{\Delta V} \sum_i D_i^6 \right), \quad (2.3)$$

where D_i is diameter of i -th scatterer and the sum is over all particles in unit volume. It follows from (2.3) that Z is heavily weighted by large particles.

Values of the reflectivity factor from volcanic ash can reach 75 dBZ in areas close to volcanic vents where large tephra particles reside. At ranges from a vent beyond 50 km, Z is low because remaining small particles in plumes produce much lower reflection according to (2.3). Dielectric permittivity of ash particles is lower than that of water. The values of $|\frac{\varepsilon-1}{\varepsilon+2}|^2$ (see eq. (2.2)) for water is 0.93 whereas for volcanic ash it is 0.36 (Harris and Rose 1983, Rose et al. 1992, Adams et al. 1996). Smaller dielectric permittivity of the ash results in weaker reflected

signals than those from rain drops. Thus, detectability of the ash is lower than that of rain or warm clouds at the same number concentration of scattering particles.

One can see from eq. (2.3) that the reflectivity factor is proportional to the sixth power of the particle's size and to the first power of number concentration. So the largest ash particles make much greater contribution to Z than do the smaller particles of equal concentrations. Larger particles fall out from the volcano plumes more quickly than small particles do. So reflectivity of ash clouds generally decreases with distance from a volcano vent. However, a secondary peak in Z is frequently observed, which is caused by condensation of volcano water vapor on ash particles and quick freezing of water droplets that produce ice crystals or snowflakes (Harris and Rose 1983).

The majority of radar observations of volcanic plumes have been made with C-band weather radars. Some historic statistics of radar observations of the ash can be found in Marzano et al (2013). Here we review some radar observations of recent eruptions conducted with C- and X-band radars. To estimate detectability of volcanic ash, we briefly review seven eruptions listed in table 2.1 and observed by radars with modern systems of digital signal processing and data archiving.

Table 2.1. Volcano eruptions observed with C- and X-band weather radars.

Eruption	Type of radar, frequency band	Distance to volcano, km	Intensity of eruption, maximal echo height
Mt Hekla, Iceland, 26-27 February, 2000	Keflavik, C-band, single pol,	144	Moderate, $H_{\max} = 12$ km
Grimsvotn, Iceland, November 2004	Keflavik, C-band, single pol.	260	Moderate, $H_{\max} = 15$ km.
Eyjafjöll, Iceland, April-May 2010	Keflavik, C-band, single pol.	156	Moderate. $H_{\max} = 10$ km.
Mt Etna, Sicily, Italy, April 2010	DPX4, X band, dual-pol	30	Weak, $H_{\max} = 6$ km.
Grimsvotn, Iceland, May 2011	DPX1, X-band, dual-pol	70	Moderate, $H_{\max} = 18$ km
Kelud, Indonesia, February 2013	C-band, single-pol	75	Intense, $H_{\max} = 22$ km
Calbuco, Chili, April 2015	RMA, C-band, dual-pol	124	Intense, $H_{\max} = 24$ km

2.1. Eruption of volcano Hekla, Iceland in February 2000

Iceland has several active volcanos (Fig. 2.1) and a number of volcanic clouds have been studied with the stationary C-band Keflavik and X-band mobile radars. Hekla volcano is located at the eastern tip of the South Iceland Seismic Zone. An eruption of Hekla in February 2000 was the first one observed by Keflavik radar located at Keflavik international airport in Iceland. The Hekla eruption on 26-27 February 2000 (Fig. 2.2) was the first event when the radar data were collected in digital format. Keflavik is a single polarization Doppler weather radar (Fig. 2.1 right) so reflectivity (Z), Doppler velocity (V), and spectrum width (W) products are available. Maximal reflectivity of 63 dBZ was observed during the eruption (Lacasse et al. 2004). Close to the volcano vent, Z is dominated by reflection from the ash but farther away snowflakes and ice crystals were formed which notably contributed to Z values. Satellite observations also showed the quick formation of ice fraction above the main volcanic ash cloud that prevented observations by the IR satellite sensors (Rose et al. 2013). An eruption onset can be detected by weather radar within a few minutes depending upon the update time of a volume coverage pattern (VCP). The direction of plume propagation can be obtained from radar as well. This is crucial information for the atmospheric transport models.

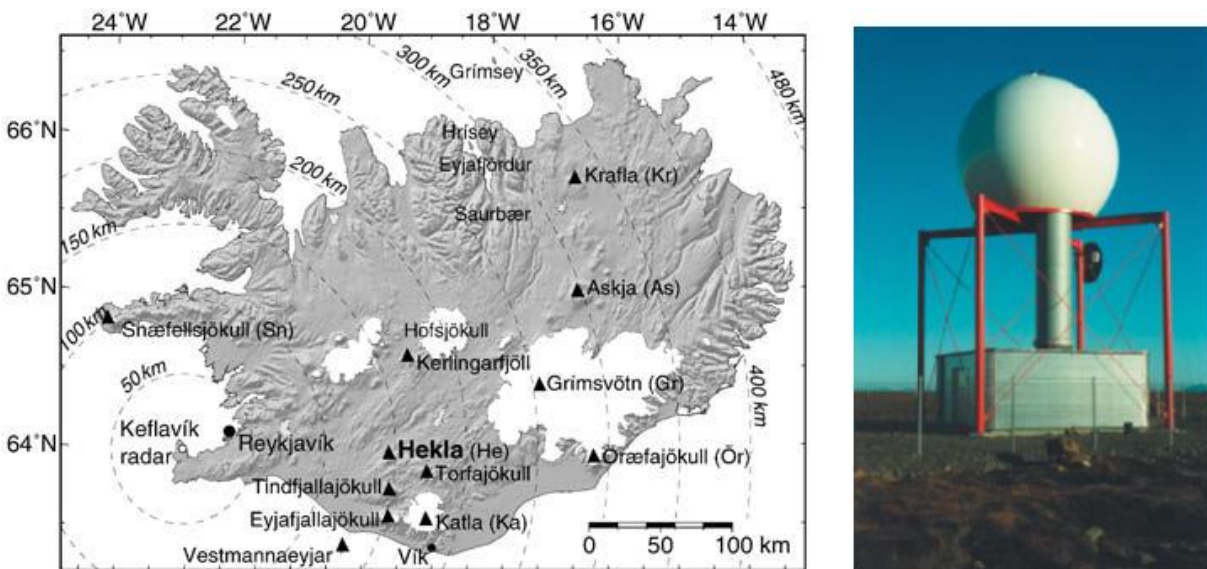


Fig. 2.1. Locations of Iceland volcanoes (left) and Keflavik radar (right). Adopted from Lacasse et al. (2004).



Fig. 2.2. Eruption of Hecla 26 February 2000 at 1835 UTC. Adopted from Lacasse et al. (2004).

Some PPI images from the volcanic plumes are shown in Fig. 2.3. The maximal distance at which radar echo from the plume was observed was about 250 km. Some snow clouds are seen to the west of the volcanic plume. A key pattern of the radar echo is seen in Fig. 2.3: the strongest reflection is above the volcano during the early eruption stage. This correlates very well with the fastest increase in the total erupted mass retrieved by IR satellite sensors (Rose et al. 2003). A region with a secondary Z maximum is located to the north from the volcano. The possible origin of this is from mixed-phase aggregation, i.e. between ice-encased or snowflake-encased ash particles (Textor et al. 2006a, 2006b). From the lowest-level PPI radar images having $Z > 30$ dBZ, one can estimate the area of both the eruption column and fallout region.

The secondary Z maximum results from water vapor in the volcanic plume. Lacasse et al. (2004) explain the high water content of the 2000 Hekla eruption with four possible origins: (1) the dissolved water content in the magma prior to eruption, (2) magmatic water which has been derived from crystallization of stored magma under the volcano, (3) the presence of groundwater within the volcano edifice, and (4) entrained ambient atmospheric humidity and resulting precipitation (e.g., snow). Ice or snow most likely began to form early within the eruption column once its temperature reached the ambient freezing temperature. The transition of water

vapor to snowflakes and ice crystals could be the origin of the secondary reflectivity enhancement down the wind.

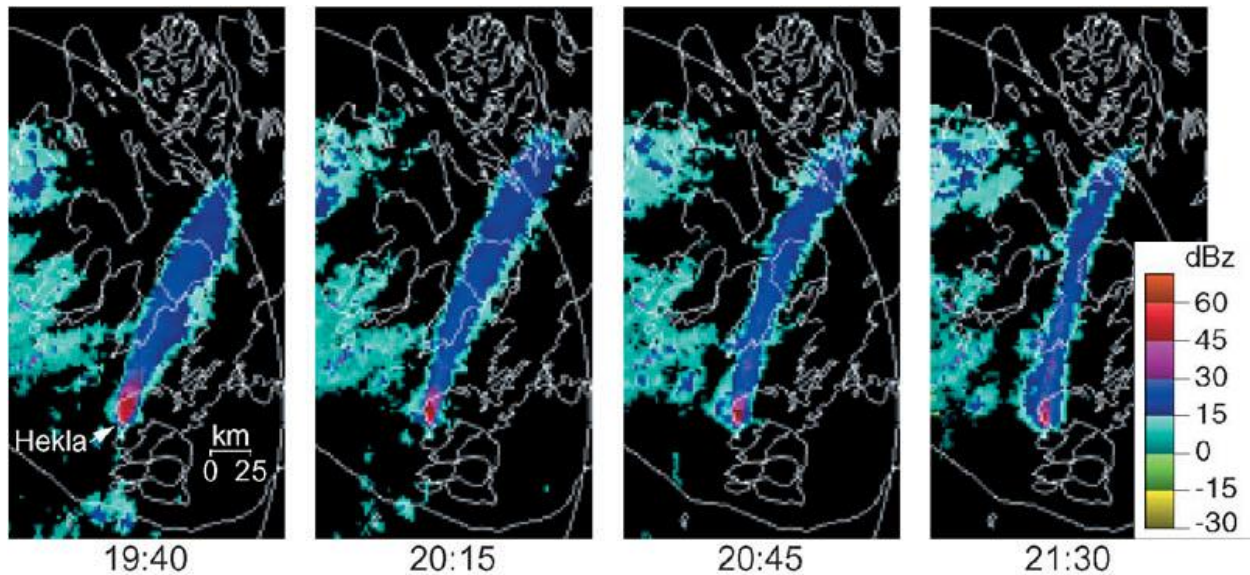


Fig. 2.3. PPI images of volcanic ash cloud from Hekla eruption on 26 Feb. 2000. Times are in UTC. The radar range ring is at 200 km. Adopted from Lacasse et al. (2004).

2.2. Eruption of Grímsvötn, Iceland on 2 November 2004

The top of the ash plume of Grímsvötn volcano (its location is in Fig. 2.1) reached a height of 15 km relative to the vent and was clearly detected by the Keflavik radar (Fig. 2.4). The maximal reflectivity values were about 25 dBZ. Actual maximal reflectivity could be larger because the lower part of radar echo from the plume was not available due to screening by terrain. Some averaging in reflectivity was also possible because of the long distance to the volcano (about 265 km).

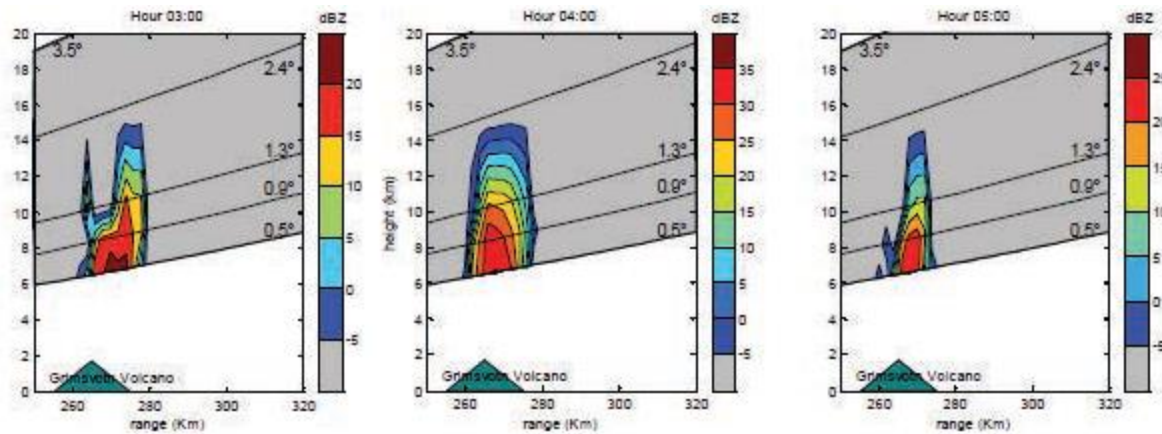


Fig. 2.4. RHI of the reflectivity factor from Keflavik C-band radar of the Grímsvötn eruption on 2 Nov 2004. The volcano vent indicated with a triangle. Adopted from Marzano et al. (2010a).

2.3. Eruption of Eyjafjöll, Iceland in April 2010

The Eyjafjöll volcano (its locations is in Fig. 2.1) awakened in April 2010. The volcano vent was under a glacier and the eruption became explosive. The eruptions occurred 14 April 2010 (Fig. 2.5) and on 15 April the ash cloud reached mainland northern Europe, thus forcing the closure of airspace (Zehner 2010). Figure 2.6 illustrates the volcano cloud observed with Keflavik weather radar (Marzano et al. 2011). The figure also demonstrates a presentation of mixed horizontal–vertical maps (also denoted as horizontal–vertical maximum intensities (HVMI)s), such that RHI reflectivity fields along the north-south and east-west directions are shown. Ground clutter is removed by signal processing and meteorological targets are identified easier. The maximal reflectivity values were around 25 dBZ.



Fig. 2.5. Volcanic clouds from Eyjafjoll volcano seen above the ice cloud deck. 14 April 2010. The top of volcanic clouds is at about 7 km. Adopted from Marzano et al. (2013).

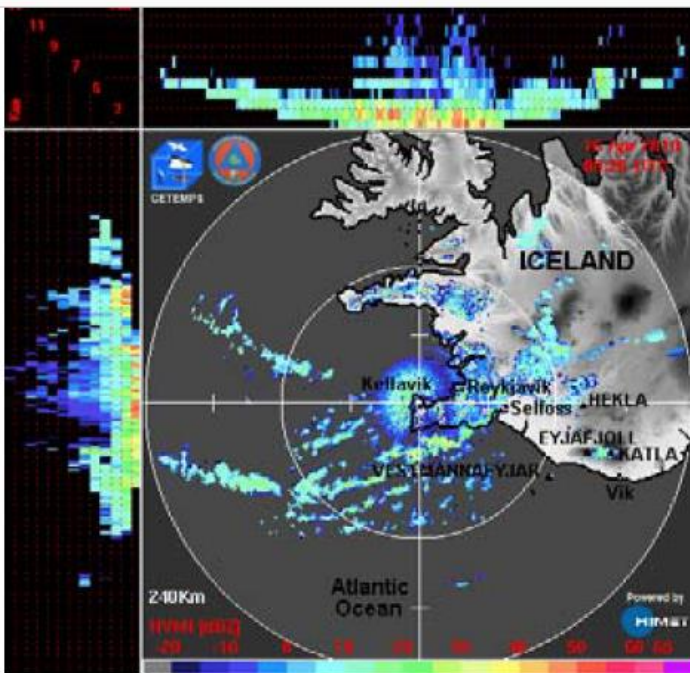


Fig. 2.6. Mixed horizontal–vertical maps of reflectivity from Keflavik radar on 14 April 2010. Adopted from Marzano et al. (2011).

2.4. Eruption of Etna, Italy in April 2011

The Mount Etna volcano is the major active European volcano, located in Sicily, Italy (Fig. 2.7). A volcanic ash cloud from an eruption on 10 April 2011, was observed by the mobile polarimetric X-band radar DPX4, located in the Catania airport area. The distance to the volcano vent is about 30 km. The radar belongs to the Italian Department of Civil Protection. It is operationally used for either weather or airborne volcanic ash monitoring. The maximal top of radar echoes from the volcanic plume was at about 6 km and the maximum reflectivity exceeded 50 dBZ near the volcano vent (Fig. 2.8).



Fig. 2.7. Location of DPX4 near Mt. Etna on 10 April 2011. Adopted from Vulpiani et al. (2011).

The DPX4 is a dual-polarization radar. A distribution of Z_{DR} values observed in the ash cloud during the eruption is shown in Fig. 2.9. One can see that the majority of values lay in an interval from -0.5 to 0.5 dB, but Z_{DR} values near the vent reach 2 dB. The specific differential phase K_{DP} was also high in the lowest layer (Fig. 2.8c). This indicates that large tephra particles are non-spherical and smaller ash particles located higher up are about spherical. The same conclusion can be drawn from the correlation coefficient ρ_{hv} : the lowest layer has low ρ_{hv} values

that point to the presence of non-spherical scatterers (Fig. 2.8d). The ρ_{hv} values increasing with height indicates more spherical particles in the upper areas.

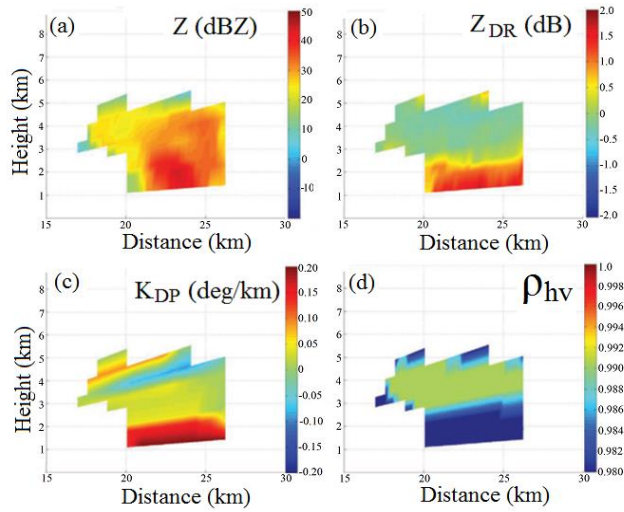


Fig. 2.8. RHI fields collected with the DPX4 on 10 April 2011 at 1330 UTC in an azimuth of 3° . Mt. Etna eruption. Adopted from Vulpiani et al. (2011).

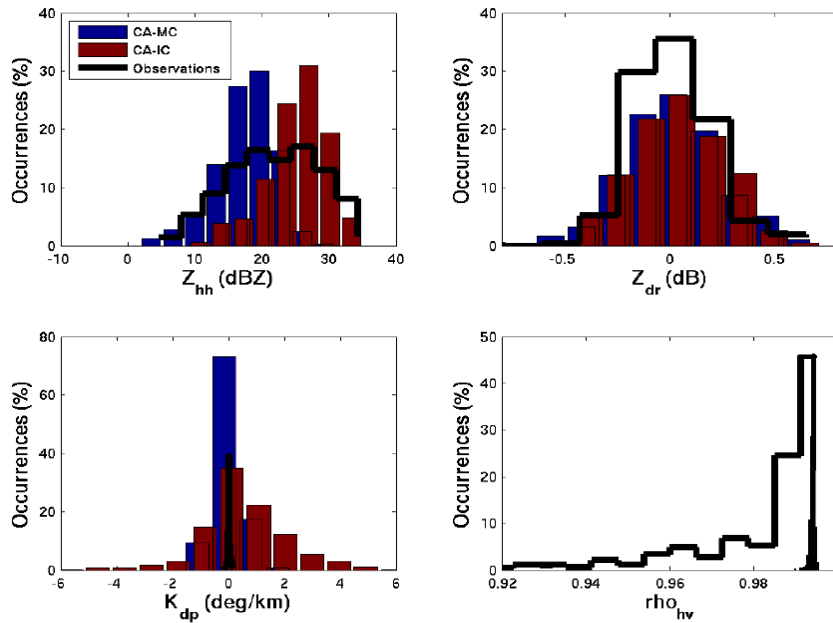


Fig. 2.9. Distributions of radar parameters (black lines) measured with the DPX4 radar on 10 April 2011, Mt. Etna case. The color histograms are the model outputs. Adopted from Vulpiani et al. (2011)

2.5. Eruption of Grímsvötn, Iceland in May 2011

This eruption occurred in May 2011 and lasted for almost 10 days. It was observed by an X-band polarimetric radar DPX1, identical to that used in the observations of the eruption of Etna in 2011 (section 2.4). The DPX1 radar was deployed 70 km from the volcano vent. An example of RHIs from the volcanic plume is shown in Fig. 2.10. The maximal reflectivity exceeded 50 dBZ at a height of about 6 km and the top of radar echo reached 20 km. A strong electrical activity was observed during this eruption. Fortunately, this plume moved northward, so that the European airspace was not affected.

The measured Z_{DR} values were mainly in an interval from -0.5 to +2 dB indicative of moderately nonspherical particles (Fig. 2.10c), where K_{DP} values were about 1-2° km⁻¹ (Fig. 2.10b). The ρ_{HV} values were sufficiently high in areas of small particles, dropping to 0.9 in the reflectivity core. Note also some areas of ρ_{HV} as low as 0.75 (Fig. 2.10d).

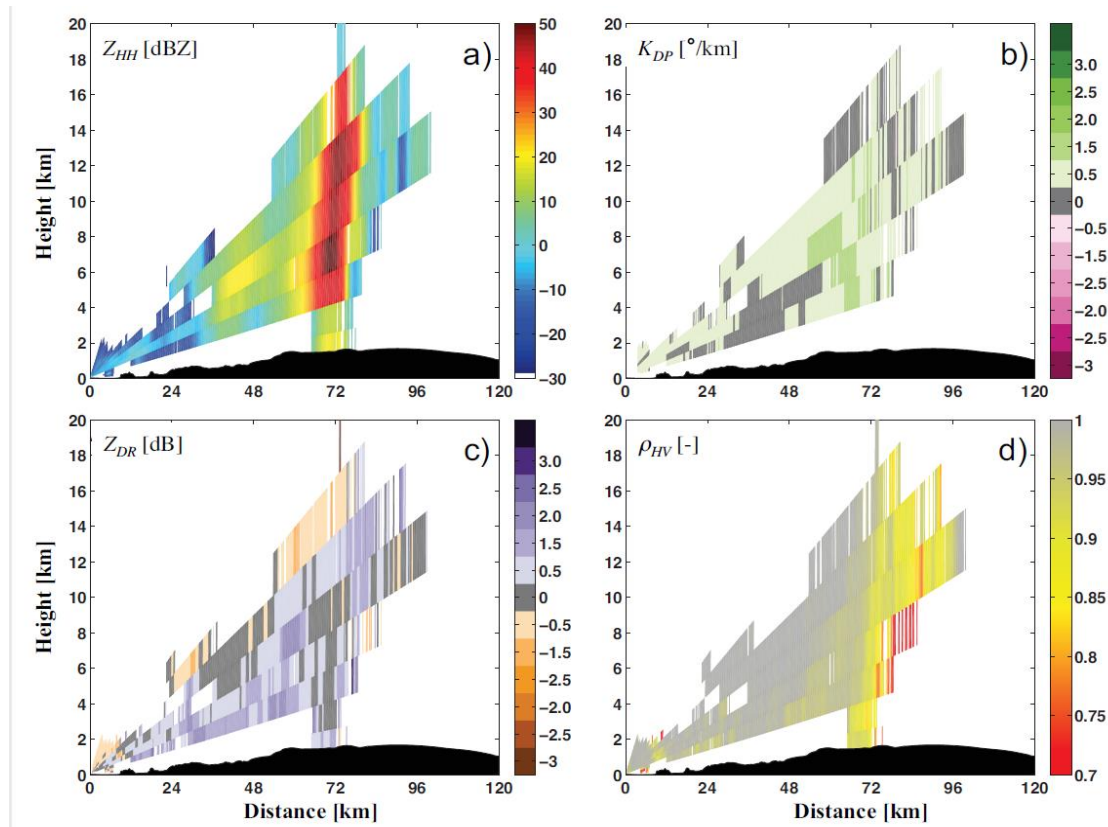


Fig. 2.10. RHIs from Grimsvotn eruption 22 May 2011, 0712 UTC, an azimuth of 21°. X-band DPX1 radar. Adopted from Montopoli et al. (2013).

2.6. Eruption of Mt Kelud, Indonesia in February 2014

Indonesia has several active volcanoes; some of them are within the range of radar operations. An example of radar observations of volcano eruption of Mt Kelud is shown in Fig. 2.11 (Wardojo 2015). The radar is a C-band non-polarimetric system. The eruption began on 13 February 2014 at 15:52 UTC. The maximal observed reflectivity was between 55 and 60 dBZ at 16:42 UTC (Mr. Wardojo did not show radar images before 16:42 UTC). Due to software limitations, the maximum heights of the ash plumes are shown up to 10 km and it is apparent from Fig. 2.11 that the plumes' top was at altitudes much higher than 10 km. It is also likely that the maximal reflectivity was stronger than 55 dBZ at times closer to the beginning of eruption.

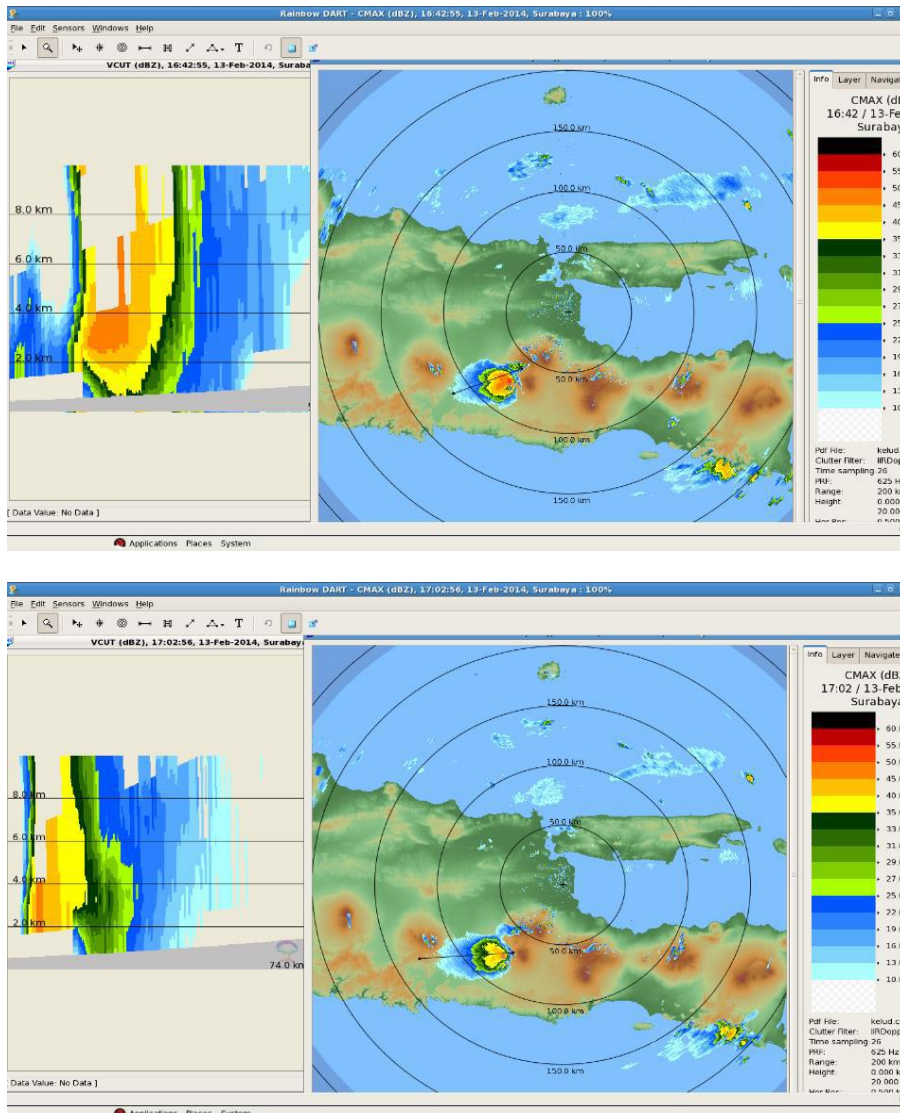


Fig. 2.11. Pseudo-RHI (right panels) and PPIs (right panels) from volcanic ash of Mt Kelud on 13 February 2014 at 16:42 UTC (top panels) and 17:02 UTC (bottom panel). Adopted from Wardojo 2015.

2.7. Eruption of Calbuco, Chili in April 2015

Calbuco volcano in Chili erupted in April 2015 (Fig. 2.12). The volcanic cloud was observed with the C-band RMA radar located in Argentina, 124 km away from the volcano (Fig. 2.13). It was a strong stratovolcanic eruption: the top of radar echoes reached 25 km and the maximal reflectivity exceeded 60 dBZ near the volcanic vent (Fig. 2.14 and 2.15). Note that the radar echo area near the vent was blocked by mountains so reflectivity of volcanic ash in areas near the ground could be larger.



Fig. 2.12. Calbuco volcano 23 April 2015. Adopted from Vidal et al. (2015).

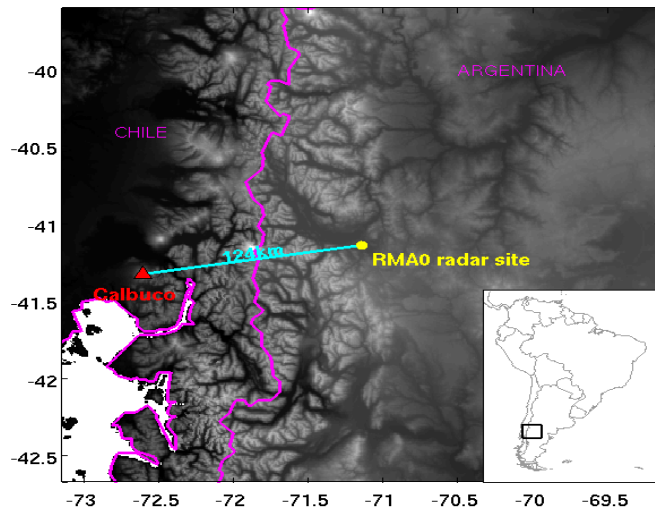


Fig. 2.13. Locations of Calbuco volcano and RMA radar. Adopted from Vidal et al. (2015).

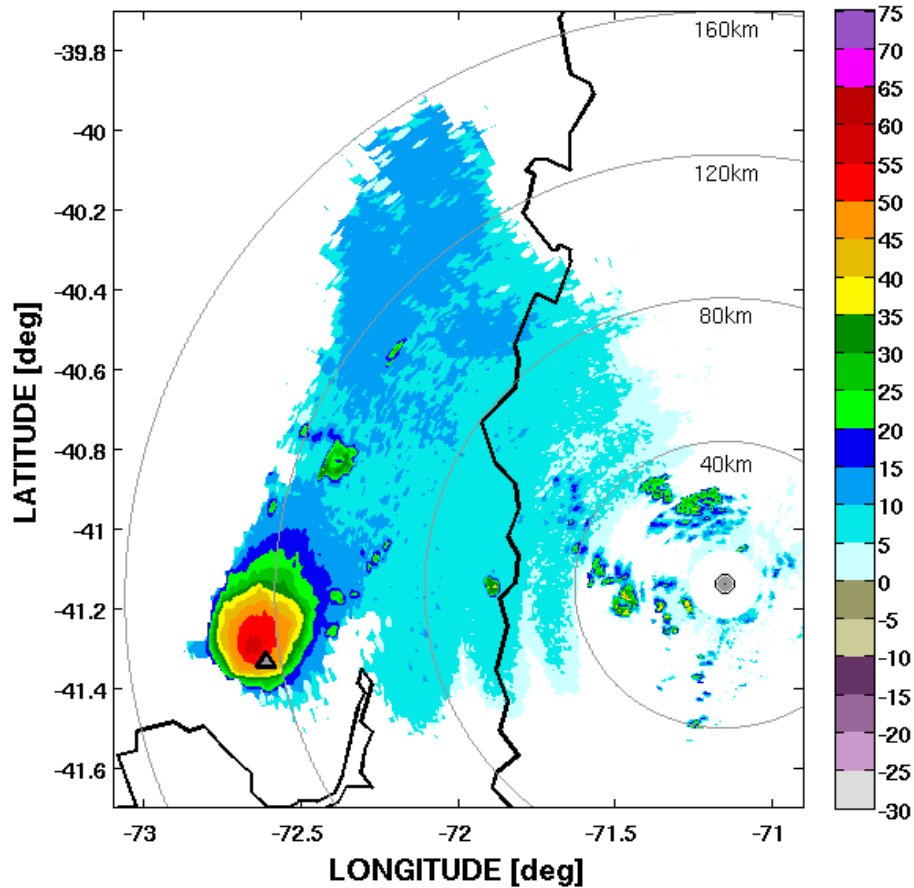


Fig. 2.14. The maximal reflectivity from Calbuco's volcanic ash observed from 0400 to 1000 UTC 23 April 2015 at an elevation of 0.5° . Adopted from Vidal et al. (2015).

Some dual-polarization RHI radar images are shown in Fig. 2.15. Values of Z_{DR} are mainly negative, and could be due to strong electrification inside the plume. Z_{DR} drops to -4 dB (Fig. 2.15 right panel) at the top of ash cloud. On the other hand, one can see an area of large positive Z_{DR} of about 2-4 dB at heights of 10-16 km. The ρ_{hv} values in this area are very low 0.3-0.5 whereas they are about 0.9 in the reflectivity core. These features point to the presence of sufficiently nonspherical and oriented ash particles at the plume's top. The common vertical orientation might be due to strong electric fields in the ash cloud. The maximal distance at which volcanic ash was observed was about 200 km.

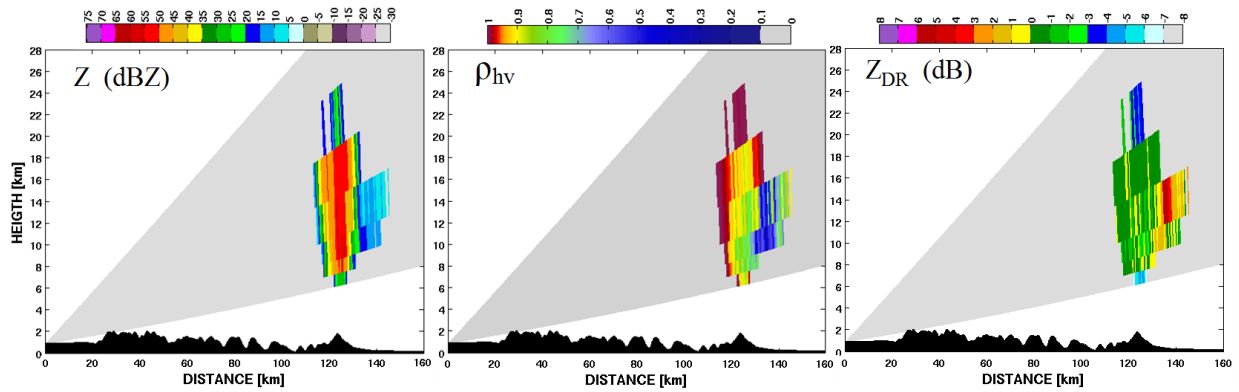


Fig. 2.15. RHI images of Z , ρ_{hv} , and Z_{DR} from volcanic ash of Calbuco eruption. 23 April 2015 at 0404 UTC. Adopted from Vidal et al. (2015).

Maximum lightning stroke rate was observed at 0715 UTC and is associated with extended coarse ash cloud located at 14km amsl. While the ash plume was growing, the main column size was diminishing (from 0500 UTC). This result is consistent with the observations by McNutt and Williams (2010). Lightning is especially vigorous when the plume was >10 km high, and this indicates that the formation of ice plays an important role in volcanic lightning.

2.8. Characteristics of radars used to observe airborne volcanic ash

A review of some volcanic eruption observed with C- and X-band radars was made in the previous subsections. Table 2.2 contains critical radar parameters necessary to assess detectability of airborne ash with those radars. The table also contains the radar parameters of two radars in the USA used for volcanic ash observations. One can see that the parameters of the C-band radars are about the same. The modern radars (RMA, Keflavik) have the radar beamwidth of about 1° , whereas the older radars had the beamwidth of 1.6° . Nowadays it is accepted that weather radars should have the beamwidth of 1° and narrower to reduce the spatial resolution and decrease effects of non-uniform beam filling that strongly affect dual polarization measurements. The pulse widths are about the same as well as the transmit powers so sensitivity of the C-band radars vary from each other by 2-5 dB. Comparisons of sensitivities of the C-band radar with that of the WSR-88D are presented in section 4.7. Here we note that the WSR-88Ds have a better sensitivity and should see volcanic ash at longer distances than those available from the radars shown in table 2.2.

Table 2.2. Parameters of C- and X-band radars used to observe volcanic ash.

	RMA,	Keflavik,	WSR-75	WR 100-22	DPX,
				EEC,	Sicily, Italy
Location	Argentina, 41.25°S/ 71.36°W	Iceland 64.01°N/ 22.38°W	Portland, Oregon, 45.36°N/ 122.36°W	Kenai, Alaska	Mobile
Polarization	Dual	Single	Single	Single	Dual
Wavelength, cm	5.6	5.5	5.6	5.6	3.2
Power, kW	350	245	230	250	Not avail.
Range, km	247	480	400	Not avail.	80
Beamwidth, deg	0.98	0.90	1.65	1.6	1.0
PRF, Hz	500	250	259	256	1875
Pulse width, μ s	2	2.2	3.0	2.0	Not avail.
VCP time, min	9	5	Not avail.	Not avail.	10

3. Observations of wild fire ash with the dual-pol WSR-88D

Smoke plumes from wild or residence fire have been observed with the dual-pol WSR-88D. Smoke plumes contain organic ash particles so their radar observations can be useful for the interpretation of radar echoes from volcanic ash. An example of probably the first observations of wild fire smoke with dual-pol WSR-88D is shown in Fig. 3.1, where radar fields of five parameters are shown, i.e., Z , V , Z_{DR} , ρ_{hv} , and Φ_{DP} . Three sources of the plumes are indicated in panel (a) with numbers 1, 2, and 3. Radar echoes from the smoke plumes were observed for several hours. Smoke from wild or residential fires contains organic ash with dielectric permittivity that can differ from that of volcanic ash. So detectability of ashes from volcanoes and fire could be different. But radar returns from wild fire smoke allows studying some dual-pol characteristics relevant to volcanic ash.

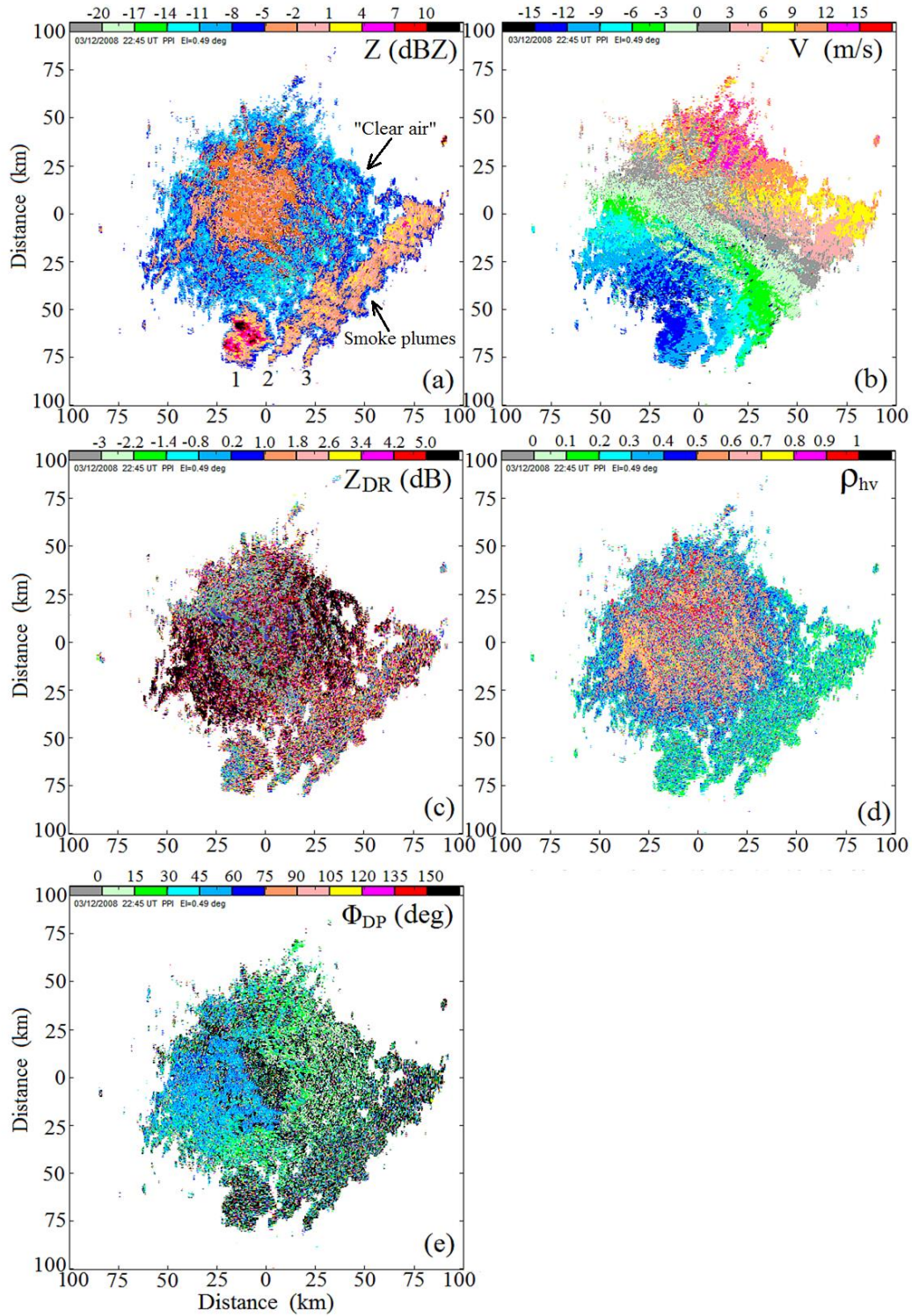


Fig. 3.1. Radar fields of “clear air” and wild fire smoke plumes observed with the WSR-88D KOUN on 03/12/2008 at 2245 UTC at an elevation of 0.5°.

As seen in Fig. 3.1(a), the plume's reflectivity factor can exceed the reflectivity factor of fair weather by 8 to 15 dB (Melnikov et al. 2008). The Doppler velocity field (Fig. 3.1b) shows that the plume is a passive tracer of the wind. The differential reflectivity values in the plumes (Fig. 3.1c) are sufficiently large and positive indicating the presence of non-spherical and horizontally oriented ash particles. The copolar correlation coefficient field shows low ρ_{hv} so the plumes can be easily distinguished from weather echoes and from Bragg scatter. Such low ρ_{hv} values also suggest that these plumes contain non-spherical particles. Small values of ρ_{hv} cause significant increase in the variance of differential reflectivity and differential phase, hence the fields of Φ_{DP} and Z_{DR} appear noisy in the region of the plume echo.

The sky at the time of radar observations was cloudy, and that allowed to comparing the dual-pol parameters from clouds and smoke plumes. Fig. 3.2 clearly demonstrates the difference in the polarimetric parameters of the plumes and clouds. Differential reflectivity of the clouds is close to 0.5 dB, whereas the plume has mostly larger Z_{DR} values with the median value of 2.8 dB. The ρ_{hv} panel shows a significant difference in the values for the clouds (0.95) and plumes (0.4). Distributions of Z_{DR} , ρ_{hv} , and Φ_{DP} for the plumes are depicted in Fig. 3.2 where the median values are 2.8 dB, 0.33, and 40° correspondingly.

The distribution of ρ_{hv} values in the plumes is very unusual for natural scatterers. Three features decrease the copolar correlation coefficient: 1) ragged shapes of scatterers, 2) randomness in their orientations and 3) a wide size distribution of particles. All of these are likely present in the observed plumes. Low ρ_{hv} demonstrate also that Bragg scatter is negligible inside the plumes.

It is seen from Fig. 3.2 that the clouds' distributions are much narrower than the plumes' ones which is a result of high ρ_{hv} in clouds. The most frequent values of Φ_{DP} are 38° and 30° in the clouds and smoke correspondingly; therefore $\Phi_{DP} = 30^\circ - 38^\circ = -8$ in smoke because $\Phi_{DP_{sys}} = 38^\circ$. Negative Φ_{DP} is unusual. The measured differential phase contains a propagation component that increases with range in a scattering media filled with horizontally aligned particles. The second contribution to the phase is the differential phase upon backscattering frequently denoted as δ . Our analysis showed no range dependence of Φ_{DP} in smoke, thus measured Φ_{DP} is solely due to the phase shift upon backscattering. The negative Φ_{DP} is caused by nonspherical particles illuminated by the two orthogonally polarized waves with differential phase in transmit ψ_t .

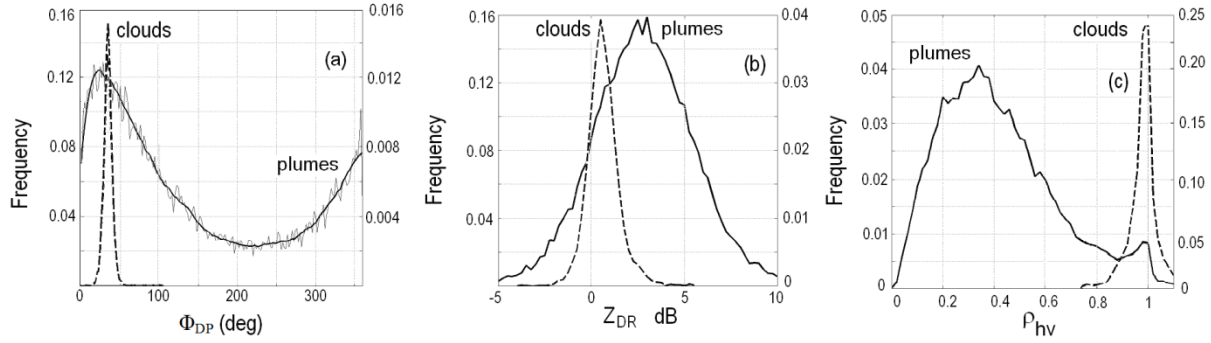


Fig. 3.2. Frequency of occurrences of radar variables from smoke (the solid curves) and from clouds (the dash curves). Adopted from Melnikov et al. (2008).

The number of radar samples M used to estimate the polarimetric parameters affects the ρ_{hv} estimates; the effect is called the statistical bias. This bias depends on M , signal-to-noise ratio (SNR), and the spectrum width. Melnikov and Zrnic (2007) showed that Z_{DR} and Φ_{DP} have negligible statistical biases but ρ_{hv} in smoke is biased significantly due to low correlations. To demonstrate this bias, two distributions of measured ρ_{hv} with $M = 128$ and 32 are depicted in Fig. 3.3. The data in smoke were collected with $M = 128$ at the pulse repetition frequency of 1013 Hz. For this dwell time, the antenna scanned a 1° sector that corresponds to the antenna beamwidth. The level 1 data were recorded, i.e., two I-Q-signals for every radar pulse in each polarimetric channels. This allows obtaining estimates with any M . For $M = 32$, the antenna scanned $\frac{1}{4}$ of the beamwidth. It is seen from Fig. 3.3 that the distributions of ρ_{hv} values and the mean values are quite different for different M . The intrinsic means of radar variables in smoke are $Z_{DR} = 2.8$ dB, $\varphi_{dp} = -8^\circ$, and $\rho_{hv} = 0.33$. The dependence of ρ_{hv} values upon the number of samples in the estimate should be taken into consideration in an analysis of dual polarization data from volcanic ash.

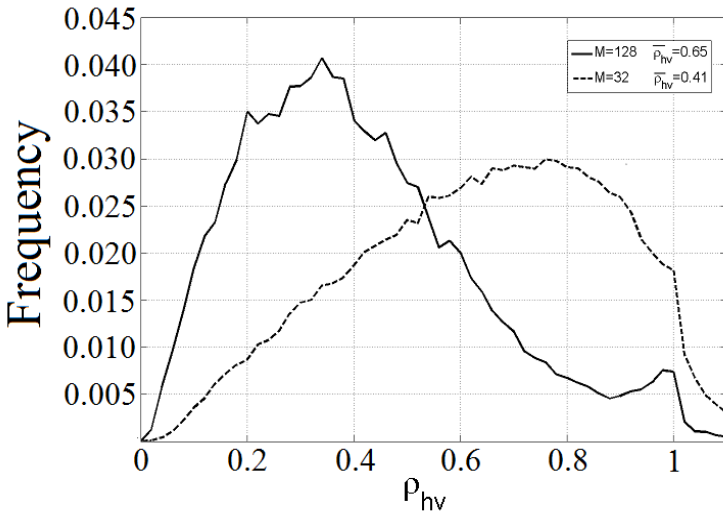


Fig. 3.3. Frequencies of occurrences of ρ_{hv} values obtained with two numbers of samples in the dwell time: $M=32$ (the dash curve) and $M=128$ (the solid curve). The data are for the smoke plumes shown in Fig. 3.1. Adopted from Melnikov et al. (2009).

4. Observations of volcanic ash with weather radars in the USA

The WSR-88Ds were upgraded to dual polarizations in 2013. There was only one significant volcanic eruption since then: the Pavlof event in Alaska which was out of the radar operational distance (section 4.6). So there have been no dual-pol WSR-88D observations of volcanic ash yet. To assess the probability of volcanic ash detection with the WSR-88Ds, we review radar observations of volcanic ash in the USA and compare sensitivities of those radars with sensitivity of the dual-pol WSR-88Ds.

Of the 169 geologically active volcanoes in the USA, 54 volcanoes have the USGS (the United States Geological Survey) threat levels of "high" or worse, based on perceived explosiveness. Table 4.1 lists 10 most dangerous volcanoes (according to USGS); some of them are in the dormant stage. Mother Nature, though, can reshuffle the ranking at any time. One can see from the table that many of these volcanoes are located close to highly populated areas in states of Washington, Oregon, and California and poses potentially high threats. Locations of the seven most dangerous volcanoes from Table 4.1 are shown in Fig. 4.1 along with the nearest WSR-88Ds.

Table 4.1. Ten most dangerous volcanoes in the USA and the nearest WSR-88Ds

	Volcano	State	Recent activity	Nearest WSR-88D, distance to the volcano, km
1	Mt St. Helens	Washington	1980	KRTX, 80 KATX, 133
2	Mt Rainier	Washington	Dormancy	KATX, 71 KRTX, 156
3	Crater Lake	Oregon	Dormancy	KMAX, 97
4	South Sister	Oregon	Dormancy	KRTX, 171 KMAX, 214
5	Mt Hood	Oregon	Early 1800s	KRTX, 71
6	Mt Shasta	California	Dormancy	KMAX, 114 KBHX, 174
7	Lassen Volcanic Center	California	1917	KBBX, 153 KRGX, 169
8	Mauna Loa	Hawaii	1984	PHKN, 58 PHWA, 32
9	Kilauea	Hawaii	1983	PHKN, 74 PHWA, 42
10	Redoubt	Alaska	2009	PAHG, 188

States of Washington, Oregon, and California comprise the first volcanic area in the USA. Alaska is the second volcanic area in this country (Fig. 4.2). Three active volcanoes in Alaska, i.e., Mt Redoubt, Mt Augustine, and Mt Spurr are located at distances of 80, 188, and 81 km correspondingly from the WSR-88D PAHG at Kenai, AK.

Hawaii is the third volcanic area in the USA, where Mauna Loa and Kilauea volcanoes are located sufficiently close to the WSR-88Ds PHKN and PHWA (Table 4.1, Fig. 4.3).

Seven explosive eruptions have been observed with weather radars in the USA (Table 4.2). The explosive stages of all eruptions have been detected with the radars; that points to their high detectability. Eruption of Anatahan volcano in April 2005 was detected at a distance of 320 km (section 4.5).

Table 4.2. Explosive volcanic eruptions in the USA observed with weather radars

Year	Volcano	Location	Radar, frequency band	Distance between volcano and radar, km	Max Z (dBZ) / Hmax (km)	Reference
1976	Augustine	Alaska	WSR-75, C-band	188	N/A	Sawada 2004
March 1982	Mt St. Helens	Washington	WSR-75, C-band	82	25 / 11	Harris and Rose 1983
August 1992	Spurr	Alaska	WSR-75, C-band	81	35 / 16	Rose et al. 1995b
April 2005	Anatahan	Mariana Islands	WSR-88D, S-band	320	>50 / ?	See the caption in Fig. 4.9.
January 2006	Augustine	Alaska	WSR-88D, S-band, Kenai	190	55 / 13.3	Marzano et al. (2010b)
March 2009	Redoubt	Alaska	WSR-88D, S-band, Kenai	80	>75/ 16	

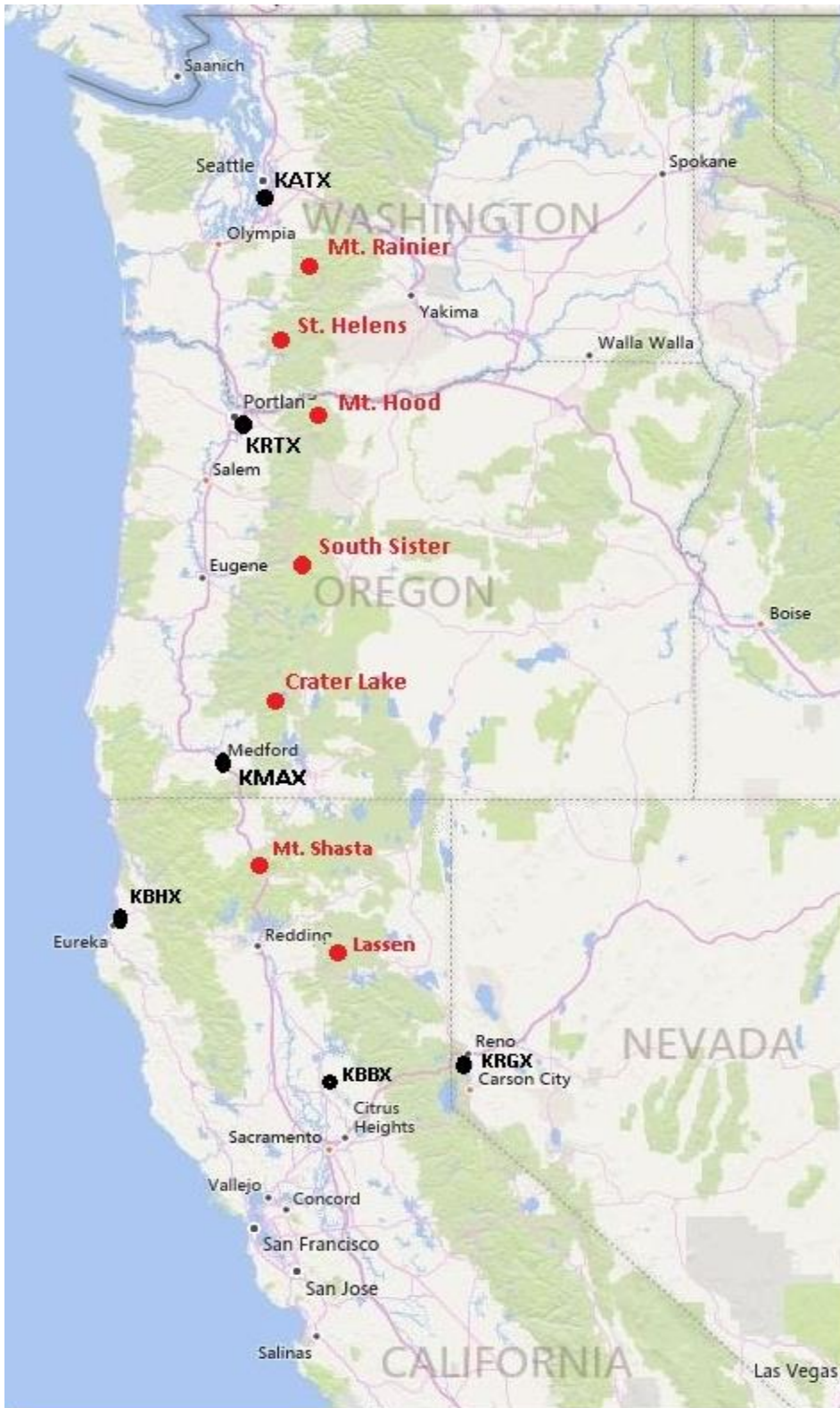


Fig. 4.1. Seven most dangerous volcanoes (red circles) and the nearest WSR-88Ds (black circles).



Fig. 4.2. Locations of volcanos Mt. Augustine, Mt. Redoubt, Mt. Spurr (red circles), and the WSR-88D PAHG at Kenai, AK (the black circle).

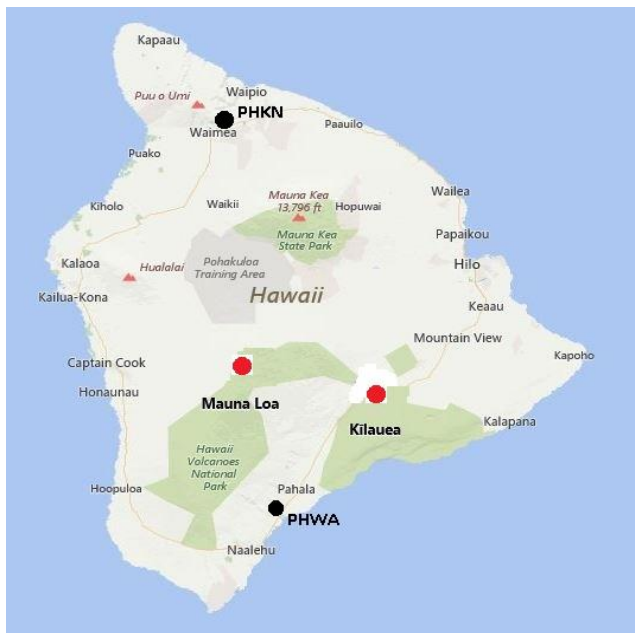


Fig. 4.3. Locations of Mauna Loa and Kilauea volcanoes (red circles) and WSR-88Ds PHKN and PHWA (black circles) in Hawaii.

The first eruption observed with a C-band radar of the US Weather Service was in 1976 (Sawada 2004). No quantitative data are available on this eruption so it is just a historic mark. The first documented observation of volcanic ash was made in 1982, which is described in the next section.

4.1. Eruption of St. Helens in March 1982

Volcano Mt St. Helens (Fig. 4.4) was active in 1980. A strong eruption begun on May 25, 1980, at 2:30 a.m. Ash cloud quickly reached 14 km. Approximately fifty-seven people were killed directly; thousands of game animals were killed, hundreds of square miles were reduced to wasteland, causing damage over \$2.89 billion (in 2015 dollars). A picture of St Helens on 18 May 1980 and a map of ash fallout from this eruption are shown in Fig. 4.4.

(https://en.wikipedia.org/wiki/1980_eruption_of_Mount_St._Helens). Unfortunately, no radar information is available on that eruption.

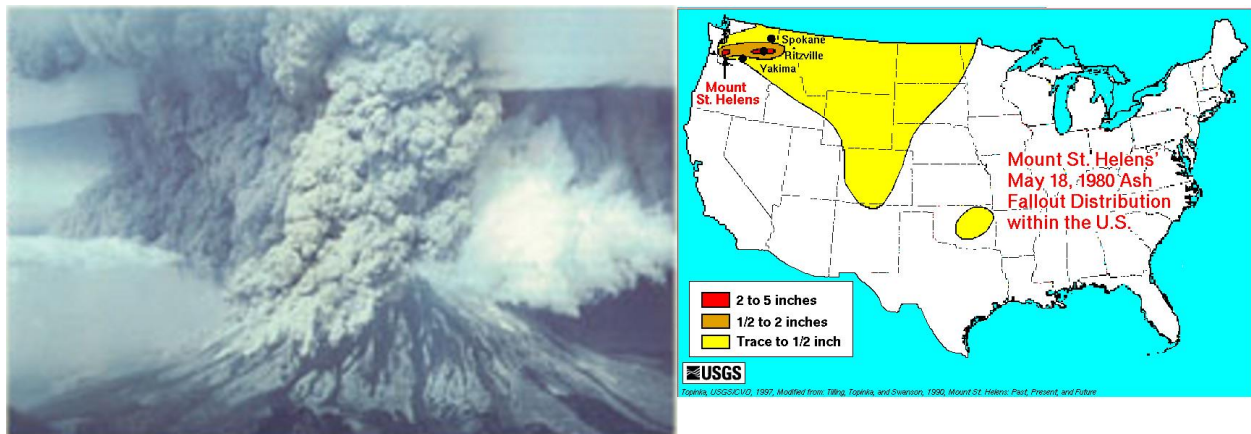


Fig. 4.4. (left): Eruption of St. Helens on 18 May 1980 and (right) the map of ash fallout from the eruption. Adopted from (https://en.wikipedia.org/wiki/1980_eruption_of_Mount_St._Helens).

An eruption on March 19-20, 1982 was a moderate one and was observed with a C-band NWS WSR-75 radar located in Portland Oregon about 82 km from the volcano. No digital images are available from those observations. Harris and Rose (1983) documented the maximum reflectivity of 25 dBZ ($272 \text{ mm}^6 \text{ m}^{-3}$) from the ash cloud.

4.2. Eruption of Mt Spurr volcano in Alaska in August - September 1992

Location of Mt Spurr volcano in Alaska is shown in Fig. 4.2. The eruptions were observed with a C-band radar (Table 4.2). A PPI and an RHI contours of reflectivity on Aug. 19, 1992 are shown in Fig. 4.5 (A,B). The maximal height of radar echoes reached 14.5 km and the maximal reflectivity was about 35 dBZ. The maximal height H_{max} (km) of radar echo is roughly connected with the eruption rate Q (kg/s) as (Rose et al. 1995),

$$H_{max} = 0.237 Q^{1/4}. \quad (4.1)$$

The constant 0.237 is an empirical number. Since radar could underestimate the ash column height because it detects the largest particles, the above equation can be used to estimate the minimal erupted amount of matter. The apparent eruption rate, estimated by the equation and integrated over the duration is about $16 \times 10^6 \text{ m}^3$, which correlates well with the amount estimated from ash fallout ($15 \times 10^6 \text{ m}^3$) (Rose et al. 1995).

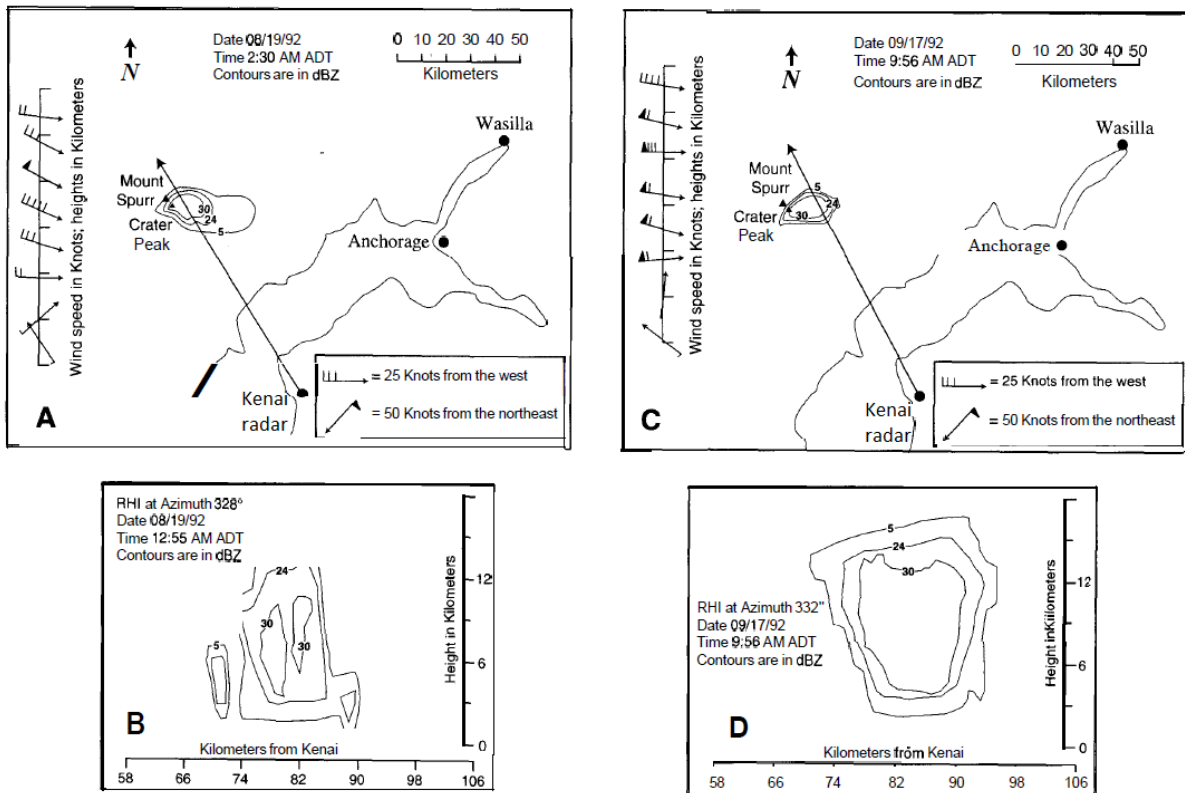


Fig. 4.5. (A): PPI reflectivity contours of eruption on 8/19/1992 at 2:30 a.m. ADT. (B): RHI reflectivity contours on the same day at 12:55 a.m. ADT. (C) and (D) same as in (A) and (B) but on 9/17/1992. The arrows in (A) and (C) show the azimuths of the RHIs shown in (B) and (D) correspondingly. Adopted from Rose et al. (1995).

The eruption of Mt Spurr on September 16, 1992 began at 10:36 a.m. ADT. A PPI and an RHI reflectivity contours are shown in Fig. 4.5 (C, D). The maximal radar echo height reached 16 km and the maximum reflectivity was estimated at 35 dBZ. The drifting ash cloud was detected by radar within distances of about 25 km from the volcano. The decrease of radar echoes was due to fallout of large ash particles from the ash cloud (Rose et al. 1995).

4.3. Eruption of Mt Augustine in January 2006

Mt. Augustine (Fig. 4.6) erupted in January 2006 several times. Some eruption events are listed in Table 4.3 along with the VCP the WSR-88D PAHG was running. The locations of the volcano and radar are shown in Fig. 4.2. Marzano et al. (2010b) analyzed radar data collected with the WSR-88D PAHG in January 2006.

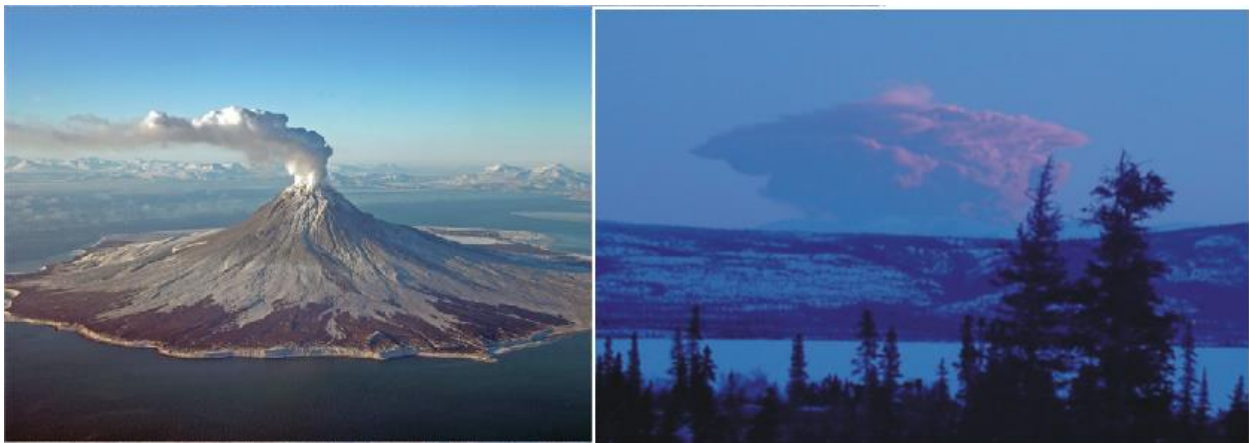


Fig. 4.6. (left): View of the east side of Augustine Island on January 24, 2006. (right): Volcanic ash cloud from Augustine. Adopted from Power et al. 2010.

Examples of reflectivity fields collected by PAHG are presented in Fig. 4.7, which correspond to event 3 in Table 4.3. Before the explosive eruption, reflectivity values in an area above the volcano vent was of around 5 to 15 dBZ, indicating that relatively small amount of ash was being emitted. The eruption began at 1324 UTC and radar reflectivity indicates a jump to 35 dBZ at 1328 UTC. At 1322 UTC, the maximal reflectivity reaches 55 dBZ at an elevation of 0.5° and 35 dBZ at an elevation of 2.4° , indicating that the volcanic plume ascended to a height of at least 10-km. The maximal reflectivity values were observed at the lowest elevation; that could be

due to largest erupted particles falling downwards. By 1345 UTC, no radar return was observed at an elevation of 2.4° , while maximum Z has decreased to 30 dBZ at at elevation of 0.5° . This drop in reflectivity indicates that the larger and more reflective particles have fallen out of the ash plume.

Table 4.3. Explosive events of Mt Augustine in January 2006 and the WSR-88Ds VCP ran during the events. PAHG radar.

Explosive event	Date and Time (UTC)	VCP
1	1/11/2006 1344	12
2	1/11/2006 1412	12
3	1/13/2006 1324	12
4	1/13/2006 1747	12
5	1/13/2006 2022	31
6	1/14/2006 0140	31
7	1/14/2006 0338	31
8	1/14/2006 0914	21
9	1/17/2006 1658	21
10	1/28/2006 0524	31
11	1/28/2006 0837	31
12	1/28/2006 1104	31

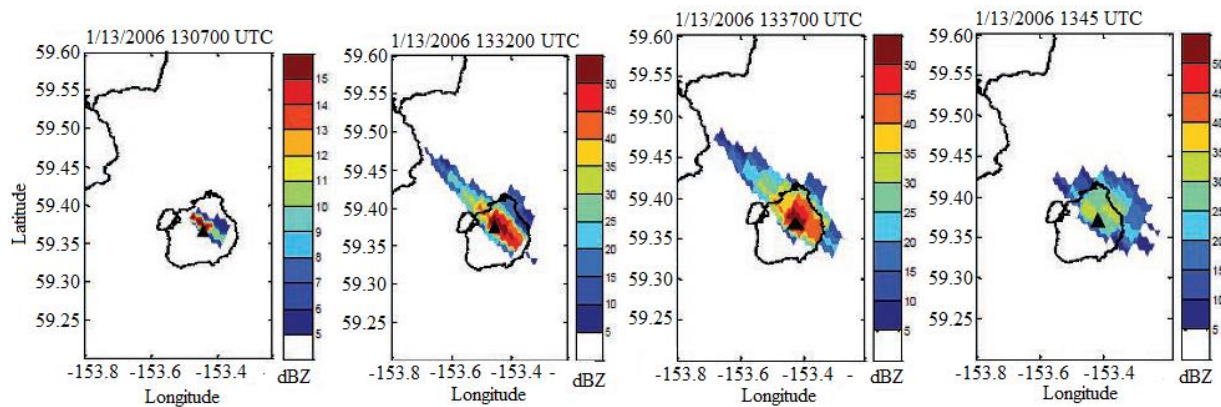


Fig. 4.7. PPI images of reflectivity of ash clouds from Mt Augustine eruption in Jan. 2006. Elevation is 0.5° . Adopted from Marzano et al. (2010b).

The rawinsonde data at 1200 UTC on 13 January 2006 indicates that -15°C isotherm was at 2.4 km. Intense freezing of water droplets condensed from erupted vapor should occur at such a temperature. The ice accretion on tephra particles should take place as well. Because dielectric permittivity of ice is lower than that for ash, reflectivity of the plume could decrease. Reflectivity can change also due to condensation of water vapor and the growth of ice crystals and snowflakes. Moreover aggregation of ash and ice particles could take place. Due to these possible processes, the interpretation of reflectivity in volcanic plumes is not straightforward.

4.4. Eruption of Mt Redoubt in 2009

The first explosion of the volcano in 2009 was recorded on March 15 and the first magmatic explosion occurred at 22:34 on March 22, 2009. Various volcanic activities continued for several months. Eruption on 23 March was well captured by the WSR-88D PAHG (Kenai, AK, Fig. 4.2, 80 km from the volcano) in a digital format. The maximal reflectivity observed on that day was stronger than 75 dB. The maximal height of radar echo was about 16 km although the top of erupted ash was visually observed up to 20 km.

There was light precipitation above the volcano at the time of eruption (Fig. 4.8). A sharp increase in reflectivity during the eruption was observed. The enhanced Z above the volcano vent was seen for about 30 minutes. Then reflectivity of volcanic ash dropped to the reflectivity of light precipitation and propagation of ash could not be traced with the radar. This event shows that the time of eruption can be observed with radar even if there is precipitation above a volcano. On the other hand, propagation of ash is difficult to trace in such a case because the ash can interact with cloud particles and precipitation. No dual-pol radar data were available at that time.

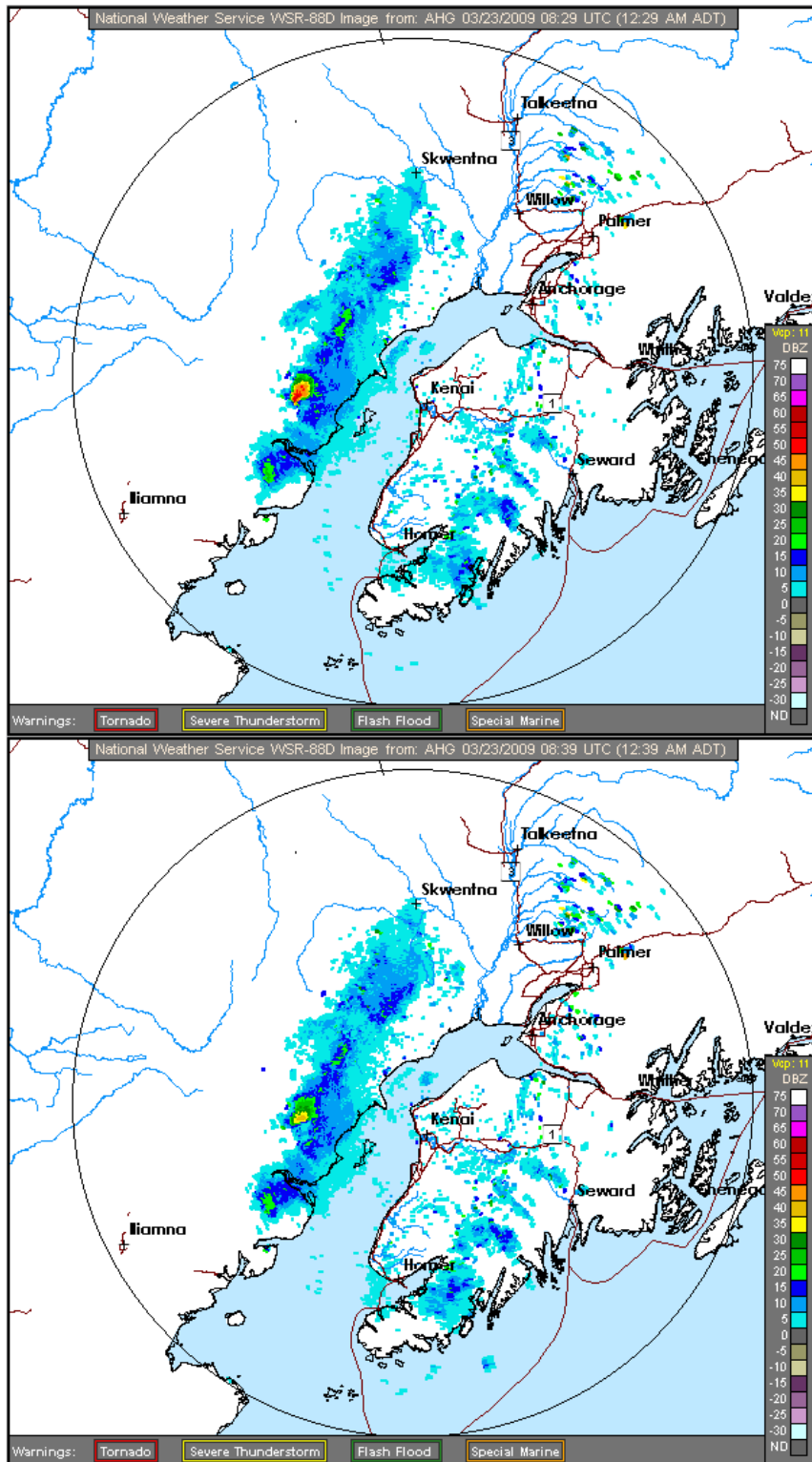


Fig. 4.8. Reflectivity fields at an elevation of 0.5° collected with the WSR-88D PAHG on 23 March 2009 at 0829 (top) and 0839 UTC (bottom).

4.5. Eruption of Anatahan in April 2005

Anatahan volcano is located on an island in the Northern Mariana Islands in the Pacific Ocean about 300 km from Guam and is an active stratovolcano (Fig. 4.9). Eruption on 5 April 2005 was captured by the GUAM WSR-88D located 320 km from the volcano (Fig. 4.9, left panel). No echo from the volcanic ash was observed at the latter time because of the long distance to the volcano. Satellite radiometers onboard GOES-9 detected volcanic plumes at large distances from the volcano (Fig. 4.9, the central and right panels). This case shows that a volcanic eruption can be observed with the WSR-88D at very long distances.

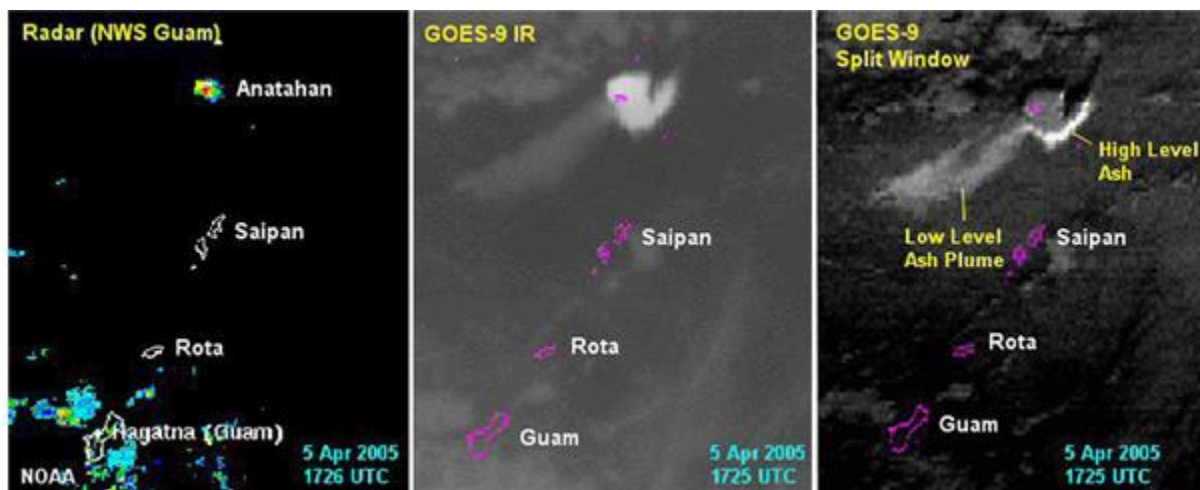


Fig. 4.9. (left): Reflectivity image from the WSR-88D at Guam. (center and right): Radiometric images from GOES-9 satellite. Adopted from http://www.meted.ucar.edu/volcanic_ash/tools/navmenu.php?tab=1&page=4.1.3

4.6. Eruption of Pavlof volcano in March 2016

Pavlof volcano erupted on 27 March 2016 at 4:18 AKDT (Fig. 4.10). The closest WSR-88D PAKC at King Salmon, AK is located 480 km away from the volcano (Fig. 4.11). The WSR-88D PABC at Bethel, AK is located 596 km from the volcano. Both distances are out of the maximal range of radar observations. A reflectivity field at an elevation of 0.5° is shown in Fig. 4.12: no echo from the volcanic ash has been observed. The ash was transported to the North from the volcano, which is seen from satellite image obtained from onboard radiometers (Fig. 4.13).



Fig. 4.10. Pavlof volcano on 27 March 2016. Adopted from <http://www.cbsnews.com/news/alaska-volcanic-eruption-creates-20000-ft-ash-plume/>

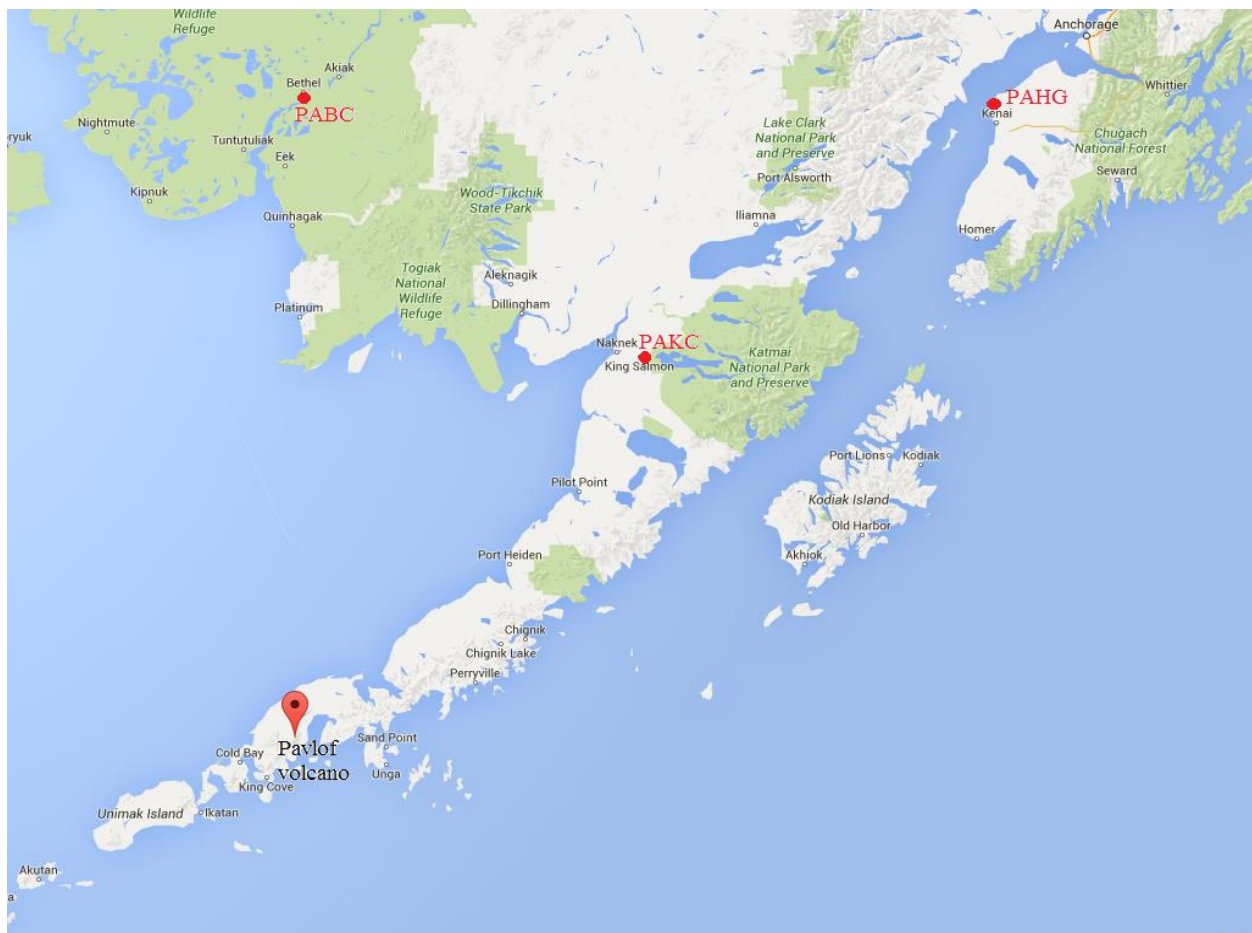


Fig. 4.11. Locations of Pavlof volcano and WSR-88Ds PAKC at King Salmon, AK, PABC at Bethel, AK, and PAHG at Kenai, AK.

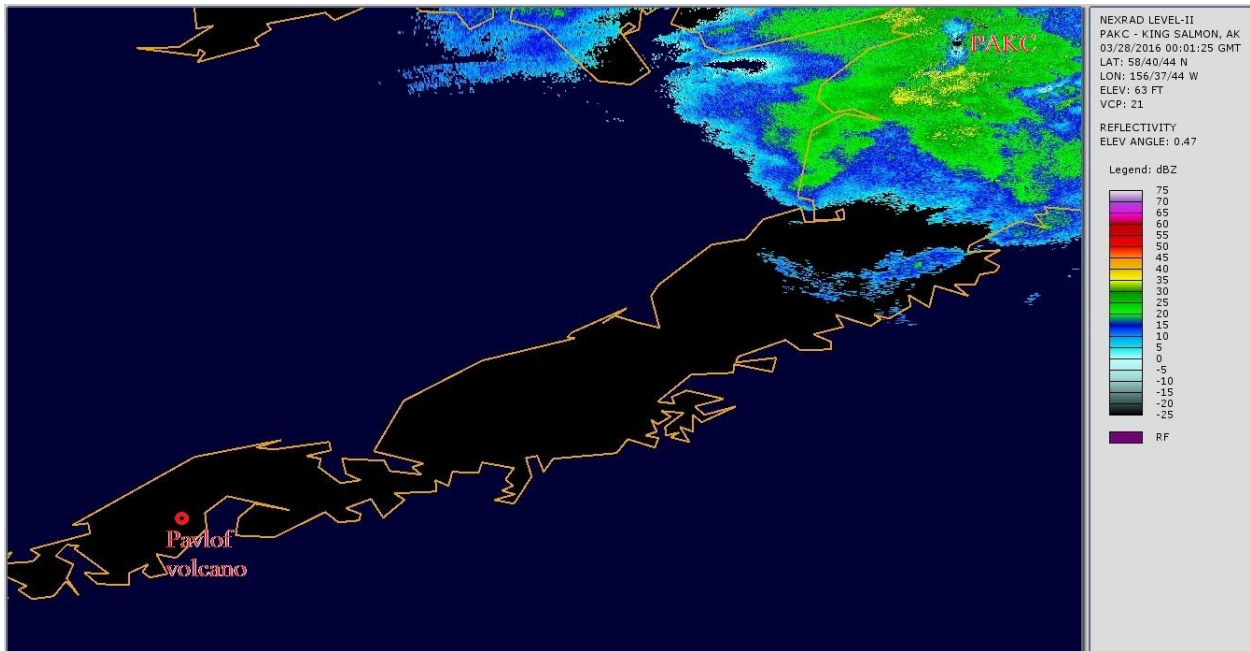


Fig. 4.12. Reflectivity image from PAKC 28 March 2016 at 0001 UTC at an elevation angle of 0.5°. Pavlof volcano, located 480 km from PAKC, is marked with the red circle.

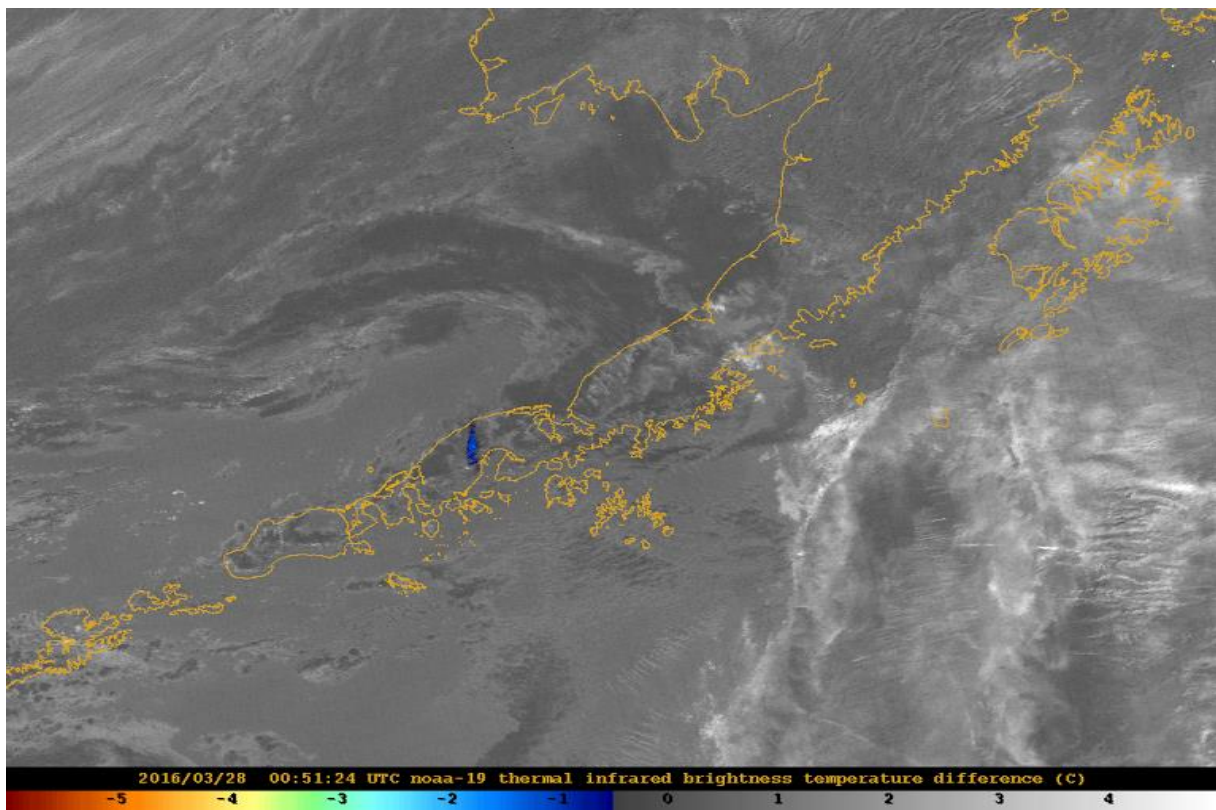


Fig. 4.13. The ash plume (the blue area) from Pavlof volcano is 45 km long. The image is from a satellite radiometer.

4.7. Comparison of radar sensitivities

The majority of radar observations of volcanic ash have been conducted with C-band systems with the wavelengths of about 5.6 cm. C-band radars can achieve better detectability of small particles than that of S-band radars due to a shorter wavelength. But C-band radars have stronger attenuation in the radar waveguides and atmosphere in comparison with that in S-band systems. Also system noise in C band systems is usually stronger than that in S band radars, and that is in favor of the latter systems. Table 4.3 lists the major system parameters of two C-band radars used to observe volcanic ash and the ones of the WSR-88D. The last entry in the table is the minimal detectable reflectivity obtained from the minimal detectable signal at a distance of 100 km. The figures for the WSR-88D was reported by Mr. Alan Free from the Radar Operations Center. One can see that detectability of the WSR-88D is better than those of Keflavik and RMA radars. Detectability of the WSR-88D is better in the long pulse mode (the pulsewidth of 4.5 microsecond) than that in the short pulse mode (1.5 microsecond) because of more energy transmitted at a narrower bandwidth. So the long pulse mode of the WSR-88Ds is preferable for observations of volcanic ash at long distances. The update time of the VCPs with the long pulse is about 10 min, which is too long for estimating the erupted ash mass. A recommended VCP is discussed in section 7.

Table 4.3. System parameters of the RMA, Keflavik, and WSR-88D radars

	RMA, Argentina	Keflavik, Iceland	WSR-88D, USA
Polarization	Dual	Single	Dual
Wavelength, cm	5.6	5.5	10 – 11
Power, kW	350	245	350
Range of observations, km	247	480	460
Beamwidth, deg	0.98	0.90	0.95
Pulse width, μ s	2	2.2	1.5; 4.5
Minimum detectable Z at R=100 km, dBZ	2	4	-2.5 (short pulse); -11 (long pulse)

A following issue should be considered in discussing of observations of volcanic ash with weather radars. The WSR-88Ds run the VCPs with update time from 5 to 10 minutes. An eruption event can last 1-2 min and it is important to measure reflectivity at lowest elevation during the eruption to estimate the amount of mass erupted. This issue is discussed in section 7.

4.8. Dual polarization properties of volcanic ash

Dual-polarization radar observations of volcanic ash are limited. Only one eruption was observed with dual pol C-band radar (Calbuco volcano, section 2.7) and two eruptions were observed with dual pol X-band radars (eruptions of Mt Etna in Italy and Grimsvotn in Iceland, sections 2.4 and 2.5).

Table. 4.4. Dual-pol parameters from volcanic and smoke plumes

Parameter	X-band radar	C-band radar	smoke plumes, S-band
Max reflectivity, dBZ	40	65	10
Differential reflectivity, dB	-0.5 to +1.5	-1.5...1.5 (Grimsvotn) -1...3 (Calbuco)	1 ... 3
Correlation coefficient	0.980 ... 0.992	0.8...1 (Grimsvotn) 0.5...1 (Calbuco)	0.3 ... 0.7
Differential phase, deg	Not available	Not available	-8
Specific differential phase, deg/km	-0.1 ... 3	0 ... 1.5 (Grimsvotn)	~0

Limited dual-pol radar data from volcanic ash do not allow for reliable conclusions. Z_{DR} values from the Etna eruption lay in an interval -1.5 to +1.5 dB, whereas Z_{DR} from Calbuco volcano lay in an interval -1 to +3 dB. The positive part of the latter Z_{DR} interval is close to values observed by the WSR-88D from wild fire smoke (Table 4.4). Negative Z_{DR} from volcanic

ash could be due to orientation of ash particles in an electric field generated in an erupted ash cloud frequently. Specific differential phase K_{DP} is significant (1.5 deg/km) in areas close to volcano vents due to the presence of large nonspherical tephra particles. Negative K_{DP} values were observed in areas of negative Z_{DR} due to vertical orientation of the ash particles.

The values of correlation coefficient (CC) are high in the Etna and Grimsvotn cases and are much smaller in the Calbuco case. This can be due to different shapes of tephra particles erupted and different number of pulses used to estimate the CC. It was shown in section 3 that the number of samples affects CC strongly: the larger the number the lower obtained CC.

The differential phase could be one of the useful parameters in the distinguishing weather and ash echoes. Measured differential phase in smoke plume was about -8° (section 3), and that is in contrast to the zero phase at the edges of weather objects. Negative phases can be observed with radars employing the simultaneous transmission scheme. The phase depends on the shape of scatterers and the system differential phase in transmit (section 3).

Marzano et al. (2012b) modelled tephra particles with oblate and prolate spheroids and calculated their polarimetric characteristics. The authors separated tephra particles by two big classes: ash and lapilli. Lapilli (singular: lapillus) means "little stones" in Latin. The size of lapilli range from 2 to 64 mm (0.08 to 2.52 in). The smaller tephra particles are called ash. The latter class is divided into two subclasses: fine ash (FA) and coarse ash (CA). Lapilli are also divided into small lapilli (SL) and large lapilli (LL). Number concentration in their model was small (SC), medium (MC), and intense (IC). Orientations and the shapes considered were tumbling (TO), oblate (OO), and prolate (PO). The calculated dual pol properties of such tephra particles are shown in Fig. 4.14.

The reflectivity values of the modelled particles can exceed 75 dBZ (panel a). Z_{DR} values lay in an interval from -1 dB to +1.5 dB, which agrees well with observations at X frequency band. Values of ρ_{hv} that are high agree with observations at X band but poorly correlates with observations at C band. The simulated K_{DP} values can be very high, which is hard to correlate with limited radar observations. The modelled properties are not in full agreement with radar observations.

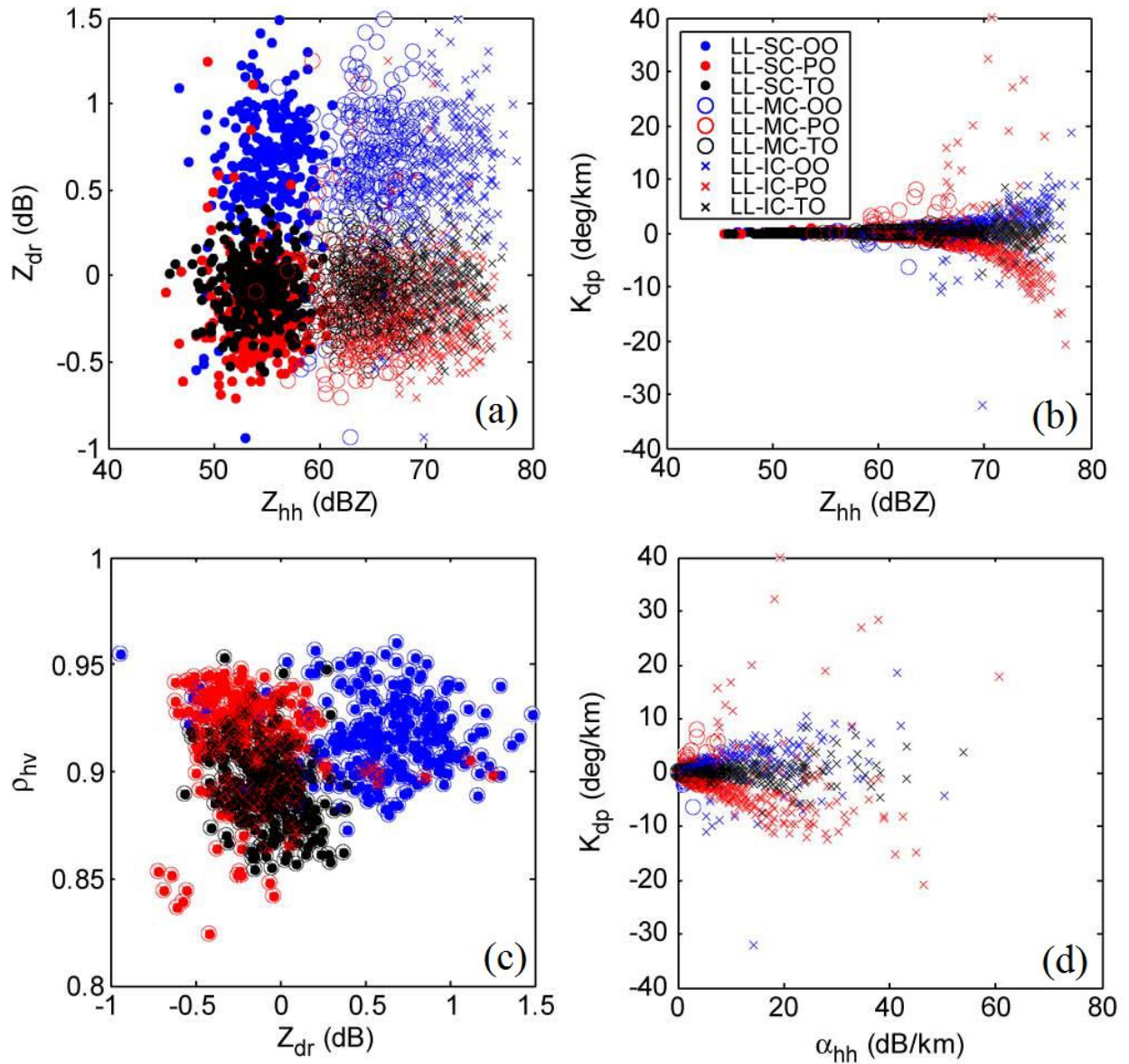


Fig. 4.14. Dual pol characteristics of tephra particles modelled as prolate and oblate spheroids. Adopted from Marzano et al. (2012b). The legend in panel (b) is explained in the text.

Integration of maximal reflectivity near a volcano vent during an eruption allows estimating the total tephra mass erupted (Marzano et al. 2013, Vulpiani et al. 2011). This is a critical input parameter for the models, which calculate transport of contaminants in the atmosphere (e.g., Webley et al. 2008). To integrate radar reflectivities, a special VCP with an update time of 0.5-1 min would be desirable.

5. Techniques to increase detectability of radar echoes

Volcanic ash in the atmosphere is a low reflecting substance at distances beyond 50 km from a volcano vent. It is important to detect ash radar echoes at long distances. Sensitivity of the dual-pol WSR-88D in Table 4.1 is for the signal level that equal system noise, i.e., for SNR = 0 dB. Some signal processing techniques are capable of detecting signals below the noise level, i.e., at negative SNR. Three such techniques are considered in this section: a) spectral processing, b) coherent summation, and c) de-speckling of radar fields.

5.1. Spectral processing to enhance detectability

Detectability of a radar echo depends on the of signal-to-noise ratio (SNR);the higher the SNR, the better the detectability. The spectral processing allows increasing the SNR. This approach is illustrated in Fig. 5.1, where the Doppler spectrum from a polarization channel is shown with the blue line. The number M of radar pulses to produce the spectrum is 128. The mean spectral noise power -is shown with the horizontal red line and has a spectral power of 0 dB, which in power units is 1. So the mean noise power is $N = M*1 = M$.

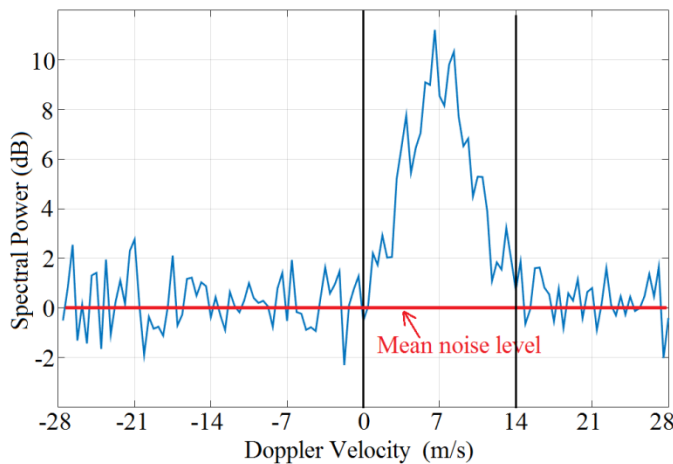


Fig. 5.1. Doppler spectrum obtained with $M = 128$. The mean spectral noise level is shown with the red line.

The spectrum from a target occupies a spectral interval of about 14 m s^{-1} , i.e., from 0 to 14 m s^{-1} , which lays in between the two vertical black lines in Fig. 5.1. The total power, i.e., signal + noise, in this interval is

$$P_{s+n} = \sum_{m=1}^{32} p_m , \quad (5.1)$$

where p_m are spectral powers in the interval $0 - 14 \text{ m s}^{-1}$, which contains 32 spectral lines. The power of signal + noise in the interval $0-14 \text{ m s}^{-1}$ is $P_{s+n} = 209.0$ in power units. The weather signal power in the spectral interval is $S = P_{s+n} - 32*1 = 177$, because the noise power in the interval is $N_o = 32*1$. So the SNR in the interval is $\text{SNR}_o = S/N_o = 177/32 = 5.5$. The total noise power in the total spectral interval (from -28 to 28 m s^{-1}) is $N=128$ and the corresponding SNR is $\text{SNR} = S/N = 177/128 = 1.4$. Compare with $\text{SNR}_o = 5.5$: SNR_o is about 4 times stronger than SNR, i.e., the spectral processing increases SNR by about 6 dB. Despite this sufficiently clear theoretical background (see also Mead 2016) no experiments with real weather radar signals have been conducted yet using this approach.

5.2. Coherent summation

SNR can be increased by the coherent summation of signals in the horizontal (H) and vertical (V) channels to increase the detection capability of the polarimetric WSR-88D (Melnikov et al. 2011). The coherent sum of voltages, e , in the H and V channels is:

$$e_{sum} = e_h + e_v = s_h + n_h + s_v + n_v , \text{ where } s \text{ and } n \text{ are weather and noise voltages}$$

correspondingly in the channels marked with the superscripts. The mean power of the sum signal is

$$P_{sum} = \langle (e_h + e_v)(e_h^* + e_v^*) \rangle = S_h + S_v + \langle s_h^* s_v \rangle + \langle s_h s_v^* \rangle + \langle n_h n_h^* \rangle + \langle n_v n_v^* \rangle , \quad (5.2)$$

where S_h and S_v are the powers of weather signal in the respective channels, the brackets define ensemble (or time) averages, the asterisk denotes complex conjugate, and the fact that the weather signal and noise voltages are zero mean and are uncorrelated is utilized. The latter equation can be written as:

$$P_{sum} = S_h + S_v + 2(S_h S_v)^{1/2} \rho_{hv} \cos(\varphi_{DP}) + N_h + N_v , \quad (5.3)$$

$N_{h,v}$ are the mean noise powers in the H and V channels respectively and φ_{DP} is the differential phase, which is one of the measurable of the DP system. Radar echoes from volcanic ash have areas with $\rho_{hv} > 0.9$. In such areas we can set $\rho_{hv} = 1$. By digitally multiplying signal in H-channel by $\exp(j \varphi_{DP})$ before coherent summation, the SNR, for the coherently summed signal can be written as,

$$SNR_{sum} = \frac{S_h + S_v + 2(S_h S_v)^{1/2}}{N_h + N_v}. \quad (5.4)$$

For equal noise powers (i.e., $N_h = N_v = N$) and SNR in each channel defined in power units as $SNR_h = S_h/N_h$, $SNR_v = S_v/N_v$, and SNR_{sum} can be written in terms of the scatterers differential reflectivity, $Z_{dr} \equiv S_h / S_v$ in power units, as

$$SNR_{sum} = \frac{1}{2} SNR_h (1 + Z_{dr}^{-1/2})^2. \quad (5.5)$$

In echoes from volcanic ash, there are areas with $Z_{dr} \approx 1$, then $SNR_{sum} \approx 2 SNR_{v,h}$. Thus the effective SNR can be increased by 3 dB. In other words, coherent summation can restore the loss of sensitivity caused by splitting the transmitted power into the H and V channels.

Fringes of radar echoes with very low SNR usually contain small droplets with $Z_{dr} \approx 1$ or ice crystals with Z_{DR} in the interval +0.5 to +2 dB, i.e., the Z_{dr} values lay in the interval 1.1 to 1.6 in power units. Using this Z_{dr} interval in (5.5) we obtain the increase of SNR_{sum} from 3 to 2 dB. This is the typical increase for the coherently summed signals.

An example of the spatial expansion of data fields, due to the SNR increase after coherent summation, is shown in Fig. 5.2 (a, b). This case shows Bragg scatter echo from optically clear air. Bragg scatter originates on fluctuations of refractivity and produces weak echoes with $Z_{DR} = 0$ dB. Properties $Z_{DR} = 0$ dB (i.e., $Z_{dr} = 1$) and $\rho_{hv} \approx 1$ for Bragg scatterers are favorable for coherent summation. The two panels in Fig. 5 show vertical cross sections of SNR in the horizontal channel (a) and SNR after coherent summation of signals in the channels (b). It is seen that echo coverage and signal intensity in panel (b) are larger than those in panel (a). Coherent summation of signals in the horizontal and vertical channels increases radar sensitivity by 2-3 dB depending on the intrinsic Z_{DR} and ρ_{hv} .

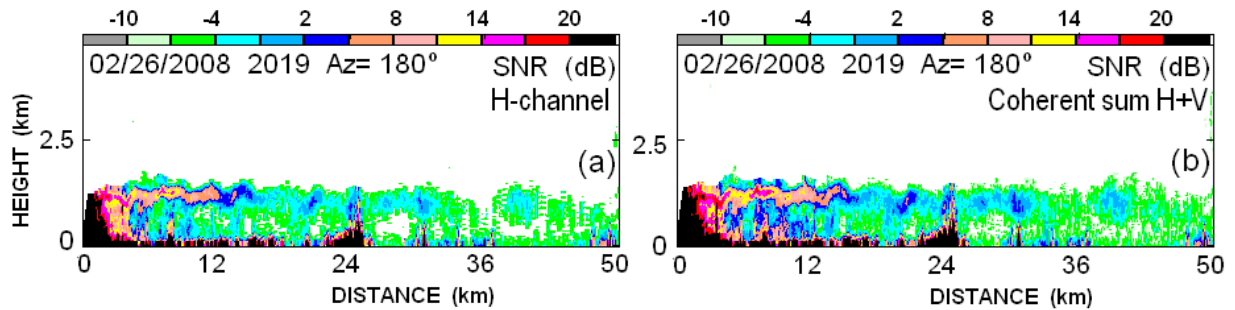


Fig. 5.2. SNR in the horizontal channel of WSR-88D KOUN. (left): Vertical cross-sections in the horizontal channel. (right): Same as in the left panel, but after coherent summation of voltages in the H and V channels. Adopted from Melnikov et al. (2011).

5.3. De-speckling of radar fields

Another technique to enhance radar detectability has been proposed by Ivic et al. (2009) that uses signal coherency in the polarimetric channels. In this subsection we consider a different approach that uses an algorithm of noise speckles removal (Melnikov and Schlatter 2011). The WSR-88D KOUN employs the SHV (simultaneous transmission of horizontally and vertically polarized waves) of polarization mode (Doviak et al. 2000). The SHV mode employs one radar transmitter so that the full transmit power is divided into two channels and the power in each channel is two times (or 3 dB) lower than the transmit power in the “legacy” single-channel system. The dual-polarization (DP) WSR-88D has a receiver for each channel similar to the one in use in the “legacy” system. Thus, the DP system in receive is the same as the “legacy” one and loss of sensitivity in the DP system equals the loss in transmit, i.e., 3 dB. The loss of sensitivity on the DP system leads to a shrinking of echo coverage, especially at long ranges from radar.

The de-speckling algorithm is based on the removal of isolated noise speckles. Probability to have noise speckles in two adjacent range gates is much lower than probability in a case of a weak radar echo. So reducing the noise threshold for radar signals and applying an algorithm that removes the speckles, it is possible to enhance detectability. A detailed description of the approach can be found in Melnikov and Schlatter (2011). The de-speckling algorithm works in a subsystem that emulates the RPG. However, the Radar Data Acquisition (RDA) subsystem is also involved in the algorithm by allowing a noisier signal to go to RPG. In other words, the RDA noise threshold should be reduced. Experiments with radar data shows that the reduction of SNR threshold can be of 5 dB, i.e., the RDA SNR threshold can be moved from +2 dB as on the “legacy” system to -3 dB with the de-speckling on. This 5 dB gain is larger than the loss of 3 dB due to power splitting that means the de-speckling restores the loss of sensitivity in the DP system.

An example of enhanced detectability using de-speckling is shown in Fig. 5.3. The figure contains two panels showing reflectivity fields collected on 20 March 2010 at 1003 UTC at an elevation of 0.5° . The left panel has been generated with the standard processing for reflectivity applying an SNR threshold of 2 dB. A reflectivity field with SNR = -3 dB obtained using the de-speckling algorithm is shown in the right panel. It is apparent that the de-speckled field has a larger coverage.

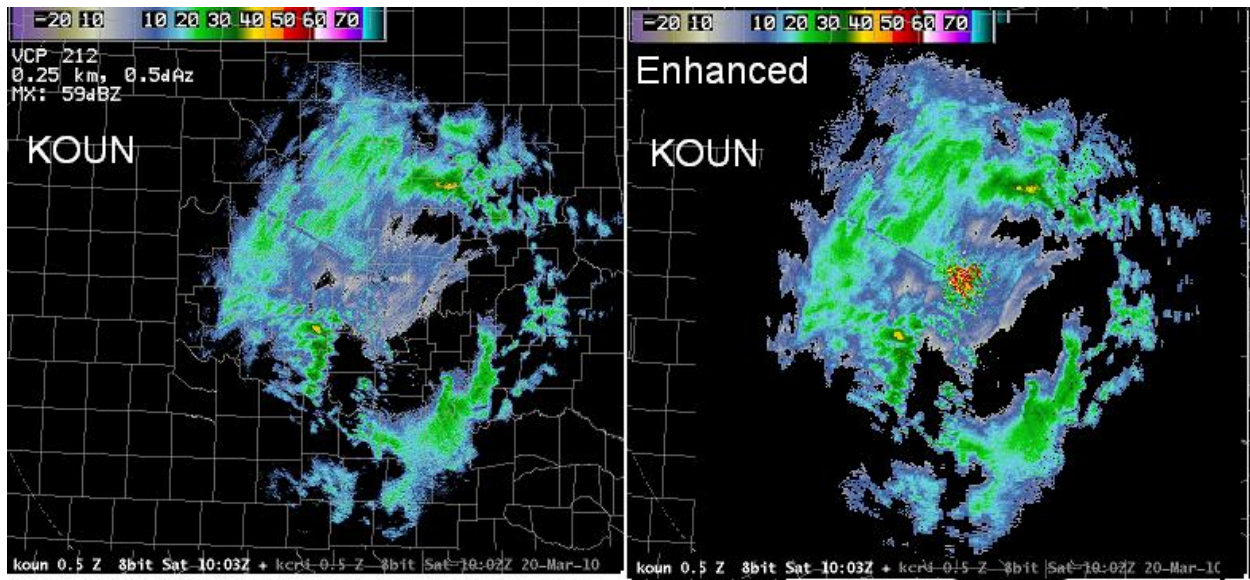


Fig. 5.3. Reflectivity from the horizontal channel of the WSR-88D KOUN. (left): Standard processing using 2 dB SNR threshold. (right): De-speckled field at SNR = -3 dB. Adopted from Melnikov and Schlatter (2011)

6. Summary

There are 169 geologically active volcanoes in the USA, from which 54 volcanoes have the USGS threat levels of "high" or worse. Seven of the most dangerous volcanoes are located close to high populated areas so the detection of possible volcanic eruption, estimation of the amount of erupted ash, and tracking ash plumes are very important. For instance, during eruption of Mt. Helens in 1982 approximately fifty-seven people were killed directly, hundreds of square miles were reduced to wasteland, causing damage over \$2.89 billion (in 2015 dollars). The USGS monitors the volcano stages and eruption events. The WSR-88Ds can be used as an additional tool to detect the time of eruption, the amount of ash erupted, and to track the volcanic plumes up to distances of 200 - 250 km.

The majority of radar observations of volcanic plumes have been made with C-band weather radars. A few eruptions were observed with the single polarization WSR-88Ds (section 4). There was just one significant eruption of Pavlof volcano in Alaska in 2016 since the WSR-88Ds were upgraded with dual polarization (2013), but the nearest WSR-88D was at a distance out of the range of radar operations (section 4.6). Sensitivity of the dual-pol WSR-88D is better than that of the C-band radars used to observe volcanic ash (Table 4.7). So the dual-pol WSR-88Ds can be used to detect an eruption event. Eruption of Anatahan volcano in April 2005 was

detected by the Guam WSR-88D at a distance of 320 km (section 4.5). All eruptions occurred within the distance of radar data collection were detected by the radars. This case points to high detectability of volcanic eruptions by the radars.

Reflectivity factor Z from volcanic ash can exceed 75 dBZ near a volcano vent. Such Z is from large tephra particles erupted. Such particles fall out of plumes at distance about 5-10 km from a volcano vent at a moderate eruption. Radar observations of volcanic plumes allow detecting the beginning of an eruption, its sustainability, and direction of dispersion in the atmosphere, i.e., three critical parameters for the atmospheric transport models.

Radar can be used to estimate the amount of ash erupted by measuring the height of the eruption column (eq. 4.1). The height of an erupted plume, determined with radar, allows estimating the amount of ash injected and forecast the location, volume, times, and propagation of ash in the atmosphere. Accuracy of this information depends on the range from radar to a volcano. Existing data allow estimating the distance of ash observation up to 200 -250 km from the WSR-88Ds.

To increase the range of observations of airborne volcanic ash, some signal processing techniques can be utilized. Spectral processing allows increasing of SNR by about 6 dB (section 5.1). Coherent summation of signals in horizontal and vertical radar channels allows increasing SNR by 2-3 dB (section 5.2). De-speckling of radar fields can decrease the SNR threshold from the current +2 dB to -3 dB, i.e., by 5 dB. There has been no work to combine these approaches to increase radar detectability, but the maximum increase of detectability can be estimated to be about 7-8 dB which would allow for the increase of tracking distance by about 30-50 km. These numbers are not so large for the monitoring of volcanic ash. So additional signal processing could be recommended for monitoring the ash when such methods are implemented in weather observations in order to increase the echo coverage.

There was no volcanic eruption in the USA since 2013, the year of dual-pol upgrade of the WSR-88Ds, in the range of the WSR-88D operations. Pavlof volcano in Alaska erupted in March 2016 (section 4.6) but the nearest WSR-88D PAKC at King Salmon, AK is located 480 km away from the volcano, i.e., out of the distance of radar data collection. So the dual pol properties of volcanic ash could not be measured with the WSR-88Ds. Some dual pol measurements are available from X- and C-band radars (section 4.8), which exhibit significant spatial and temporal variations that points to the processes of fallout, aggregation, and

sublimation of tephra particles, volcanic gases, and atmospheric vapor and ice crystals. Differential reflectivities span an interval from -1.5 dB to +3 dB: largest Z_{DR} and K_{DP} values have been observed in areas just above the volcanic vents that points to the presence of large non-spherical tephra particles. Z_{DR} and K_{DP} decrease with the distance from the vents which is a result of the fallout of largest particles from volcanic plumes. In some plume areas Z_{DR} is negative; this could be caused by strong electric fields that orient the particles vertically.

The correlation coefficients (CC) values measured at X band are larger than 0.98 whereas at C band, the values lie in a wide interval of 0.5 – 1.0. Smallest values have been measured in areas close to the volcanic vent, i.e., where the largest non-spherical particles reside. The CC measurements depend on number of radar samples used in the estimation (section 3). This number is not available from published documents so the reported CC values should be taken with caution. The polarimetric properties of wild fire plumes exhibit positive Z_{DR} (1-3 dB) and CC values in an interval 0.3 - 0.7 measured with the number of samples larger than 32 (section 3). Higher CC values in volcanic ash could be due to more spherical particles there than those in wild fire smoke. Differential phase values in volcanic ash have not been documented. In wild fire smoke, the differential phase can be negative (Table 4.4) that is due to the prolate shape of the particles and radar differential phase in transmit (section 3).

Maximal reflectivity from volcanic ash depends on the intensity of an eruption and varies from 30 dBZ to more than 75 dBZ (e.g., Mt Redoubt, 2009). This parameter correlates well with the rate of eruption. Time integration of this rate allows estimating the total amount of erupted tephra (the end of section 4.8). The amount of erupted tephra is a critical parameter for models, which calculate the transport of contaminants in the atmosphere. To integrate reflectivity in areas close to a volcanic vent, a VCP with a decreased update time at low elevations is needed. Such a VCP should have an update time of 0.5-1 min at low elevations because eruptions can last 1 -2 min and the current “clear air” long-pulse VCP has an update time of 10 min. A recommended VCP is discussed in section 7.

7. Recommended VCPs for radar observations of volcanic ash

To observe weather with the WSR-88D radars, several volume coverage patterns (VCPs) have been designed. The major issues with radar observations are conflicting requirements on data quality and the update time. A high data quality requires a large number of radar samples to

be averaged, which increases the dwell time and correspondingly reduces the update time. The update time is critical for revealing the dynamics of weather objects, especially severe weather. The same problem exists in observations of volcanic plumes: to estimate the ash mass erupted, radar data of good quality and an update time of about 2 min at the lowest elevation are needed. Tracking of the evolution of a volcanic ash radar echo is important for estimating the rate with which volcanic ash pollutes the atmosphere.

The WSR-88Ds are capable of operating in two pulse modes; the short pulse (a duration of 1.5 μ s) and the long pulse (a duration of 4.5 1.5 μ s). When using the long pulse, radar sensitivity is better by 9 dB than in the short pulse mode. Therefore, detectability of radar echoes is better when using the long pulse mode. A pulse repetition frequency (PRF) in the long pulse mode is lower than that in the short pulse mode because the total transmitting energy is limited. A lower PRF makes the observations in the long pulse mode longer in comparison with the short pulse mode. Better detectability of the long pulse mode is preferable for observations of volcanic plumes at long distances from radar, but a low PRF leads to a long update time. A VCP with the long pulse and an update time of 5-6 min is desirable for observations of volcanic ash at distances beyond 200 km.

Ash particle size distribution and the total ash mass in the atmosphere estimated from radar data are not so reliable at this time because of small amount of data available. Dual-polarization technology is a promising tool for that, but the application of this technology to volcanic ash is in a preliminary stage. Therefore it is recommended to get a more rapid update of radar data with reduced data quality. Two VCPs could be used to observe volcanic ash at distances within and beyond a distance of 200 km from radar.

At distances within 200 km from radar, VCP-212 (Fig. 7.1) is recommended to observe volcanic ashes in the short pulse mode. This VCP contains 14 tilts with the maximum elevation of 19.5° and the update time of about 4.6 min. Option AVSET is recommended to be ON, which allows completing the VCP at a lower elevation angles if there is no radar echoes. Option SAILS should also be ON, which allows for more rapid update at elevation of 0.5° to observe volcanic ash close to the ground. This VCP has the maximum elevation of 19.5° therefore it is capable of detecting the tops of volcanic plumes so the intensity of an eruption can be estimated from the maximal height of radar echoes. The erupted mass can be estimated from this height as well (see

Eq. (4.1) in section 4.2). Therefore, VCP-212 with active options “AVSET” and “SAILS” is considered as a good choice for radar observations of volcanic ash at this time.

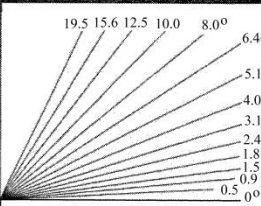
Quick Reference VCP Comparison Table for RPG Operators as of RPG Build 18						July 2016
Slices	Tilts	VCP	Time*	Algs.	Usage	Limitations
	14	12	4.3 mins	AVSET	Fastest VCP. Rapidly evolving, severe convective events (e.g. squall line, MCS).	High antenna rotation rate decreases the effectiveness of clutter filtering and decreases the accuracy of the base data estimates.
		212	4.6 [†] mins	SAILS MRLE	Rapidly evolving, severe convective events (e.g. supercells, squall line, MCS). Uses SZ-2 to significantly reduce range-obscured V/SW data compared to VCP 12.	All Bins clutter suppression is not recommended. High antenna rotation rate decreases the effectiveness of clutter filtering and decreases the accuracy of the base data estimates. PRF sectors not allowed.

Fig. 7.1. Specifications of VCP-12 and VCP-212 for the WSR-88Ds.

At distances beyond 200 km from radar, a VCP using the long pulse mode is desirable. The WSR-88D has VCP-31 with the update time of 10 min, which is too long for observations of volcanic ash. When observing volcanic ash, Doppler velocity data can be considered as secondary information since the ash appears as passive contaminants that can be tracked by observing time evolutions of their echoes. So the Doppler scans in VCP-31 could be omitted and the surveillance scans retained. VCP-31 has 5 elevations (0.5, 1.5, 2.5, 3.5, and 4.5°) with a scan time of 71.78 sec at each elevation angle, so the update time could be reduced to 6 min for such a modified VCP-31. This is an acceptable time for observations at long distances.

References

- Adams, R. J., Perger, W. F., Rose, W. I. and Kostinski, A. 1996: Measurements of the complex dielectric constant of volcanic ash from 4 to 19 GHz. *J. Geophys. Res.* **101**, 8175-8185.
- Cadle, R. D., A. L. Lazrus, B. J. Huebert, L. E. Heidt, W. I. Rose, D. C. Woods, R. L. Chuan, R. E. Stoiber, D. B. Smith and R. A. Zielinski, 1979: Atmospheric implications of studies of Central American volcanic eruption clouds. *J. Geophys. Res.*, **84**, 6961-6968.
- Cantor, R., 1998: Complete avoidance of volcanic ash is the only procedure that guarantees flight safety. *ICAO J.*, **53**, 18-19.
- Casadevall, T. J., Ed., 1994: Volcanic ash and aviation safety: *Proceedings of the First International Symposium on Volcanic Ash and Aviation Safety*. USGS Bull. 2047, 450–469.
- Donnadieu, F., 2012: Volcanological applications of Doppler radars: A review and examples from a transportable pulse radar in L-band. *Doppler Radar Observations: Weather Radar, Wind Profiler, Ionospheric Radar, and Other Advanced Applications*, J. Bech and J. L. Chau, Eds., InTech, 409–446.
- Doviak, R.J., V. Bringi, A. Ryzhkov, A. Zahrai, D. Zrníc, 2000: Considerations for polarimetric upgrades to operational WSR-88D radars. *J. Atmos. Oceanic Technol.*, **17**, 257 – 278.
- Graf, H. F., Q. Li, and M. A. Giorgetta, 2007: Volcanic effects on climate: Revisiting the mechanisms. *Atmos. Chem. Phys.*, **7**, 4503–4511.
- Harris, D. M., and W. I. Rose Jr., 1983: Estimating particle sizes, concentrations, and total mass of ash in volcanic clouds using weather radar. *J. Geophys. Res.*, **88** (C15), 10969–10983.
- Herzog, M., H.-F. Graf, C. Textor, and J. M. Oberhuber, 1998: The effect of phase changes of water on the development of volcanic plumes. *J. Volcanol. Geotherm. Res.*, **87**, 55–74.
- Ivić, I. R., D. S. Zrníc, Tian-You Yu, 2009: The use of coherency to improve signal detection in dual-polarization weather radars. *J. Atmos. Oceanic Technol.*, **26**, 2474–2487.
- Kitchen, M., and P. M. Jackson, 1993: Weather radar performance at long range—Simulated and observed. *J. Appl. Meteor.*, **32**, 975–985.
- Lacasse, C., S. Karlsdottir, G. Larsen, H. Soosalu, W. I. Rose, and G. G. J. Ernst, 2004: Weather radar observations of the Hekla 2000 eruption cloud, Iceland. *Bull. Volcanol.*, **66**, 457–473.

- Maki, M., K. Iwanami, R. Misumi, R. J. Doviak, T. Wakayama, K. Hata, and S. Watanabe, 2001: Observation of volcanic ashes with a 3-cm polarimetric radar. *Proc. 30th Int. Conf. on Radar Meteor.*, Munich, Germany, Amer. Meteor. Soc., P5.13. online https://ams.confex.com/ams/30radar/techprogram/paper_21897.htm.
- Marzano, F. S., S. Barbieri, G. Vulpiani, and W. I. Rose, 2006a: Volcanic cloud retrieval by ground-based microwave weather radar. *IEEE Trans. Geosci. Remote Sens.*, **44**, 3235–3246.
- Marzano, F. S., G. Vulpiani, and W. I. Rose, 2006b: Microphysical characterization of microwave radar reflectivity due to volcanic ash clouds. *IEEE Trans. Geosci. Remote Sens.*, **44**, 313–327.
- Marzano, F. S., S. Barbieri, E. Picciotti, and S. Karlsdottir, 2010a: Monitoring subglacial volcanic eruption using C-band radar imagery. *IEEE Trans. Geosci. Remote Sens.*, **58**, 403–414.
- Marzano, F. S., S. Marchiotto, C. Textor, and D. Schneider, 2010b: Model-based weather radar remote sensing of explosive volcanic ash eruption. *IEEE Trans. Geosci. Remote Sens.*, **48**, 3591–3607.
- Marzano, F. S., 2011: Remote sensing of volcanic ash cloud during explosive eruptions using ground-based weather radar data processing. *IEEE Signal Process. Mag.*, **28**, 124–126, doi:10.1109/MSP.2010.939846.
- Marzano, F. S., M. Lamantea, M. Montopoli, S. Di Fabio, and E. Picciotti, 2011: The Eyjafjoll explosive volcanic eruption from a microwave weather radar perspective. *Atmos. Chem. Phys.*, **11**, 9503–9518.
- Marzano, F. S., M. Lamantea, M. Montopoli, B. Oddsson, and M. T. Gudmundsson, 2012a: Validating subglacial volcanic eruption using ground-based C-band radar imagery. *IEEE Trans. Geosci. Remote Sens.*, **50**, 1266–1282.
- Marzano, F. S., E. Picciotti, G. Vulpiani, and M. Montopoli, 2012b: Synthetic signatures of volcanic ash cloud particles from X-band dual-polarization radar. *IEEE Trans. Geosci. Remote Sens.*, **50**, 193–211.
- Marzano, F.S., E. Picciotti, M. Montopoli, and G. Vulpiani, 2013a: Inside Volcanic Clouds. Remote Sensing of Ash Plumes Using Microwave Weather Radars. *BAMS*, October, 1567 – 1586.

- Marzano, F. S., M. Lamantea, M. Montopoli, M. Herzog, H. Graf, and D. Cimini, 2013b: Microwave remote sensing of the 2011 Plinian eruption of the Grimsvotn Icelandic volcano. *Remote Sens. Environ.*, **129**, 168–184.
- Mead, J.B., 2016: Comparison of meteorological radar signal detectability with noncoherent and spectral-based processing. *J. Atmos. Ocean. Technol.*, **33**, 723-739.
- Melnikov, V.M., and D.S. Zrnic, 2007: Autocorrelation and cross-correlation estimators of polarimetric variables. *J. Atmos. Oceanic Technol.*, **24**, 1337-1350.
- Melnikov, V., D. Zrnic, R. Rabin, and P. Zhang, 2008: Radar polarimetric signatures of fire plumes in Oklahoma. *Geophys. Res. Letters*, **35**, doi:10.1029/2008GL034311.
- Melnikov, V., D. Zrnic, and R. Rabin, 2009: Polarimetric radar properties of smoke plumes: A model. *J. Geophys. Res.*, 114, D21204, doi:10.1029/2009JD012647.
- Melnikov, V., P. T. Schlatter, 2011: Enhancing sensitivity on the polarimetric WSR-88D. *27th Conference on Interactive Information and Processing Systems (IIPS)*, Seattle, WA, AMS, 14.3. <http://ams.confex.com/ams/91Annual/webprogram/Paper178856.html>.
- Melnikov, V.M., R. J. Doviak, D. S. Zrnic, and D. J. Stensrud, 2011: Mapping Bragg scatter with a polarimetric WSR-88D. *J. Atmos. Oceanic Technol.*, **28**, 1273-1285.
- Mereu, L., S. Marzano, M. Montopoli, and C. Bonadonna, 2015: Retrieval of terpha size spectra and mass flow rate from C-band radar during the 2010 Eyjafjallajokull eruption, Iceland. *IEEE Trans. Geosci. Remote Sens.*, **53**, 5644 – 5660.
- Montopoli, M., M. Herzog, G. Vulpiani, D. Cimini, F.S. Marzano, and H. Graf. Remote sensing of volcanic ash: Sinergistic use of ash models and microwave observations of the eruptive plumes. *IGARSS-2013*, 717 - 714.
- Power, A., M.L. Coombs, and J. T. Freymuller, 2010: The 2006 Eruption of Augustine Volcano, Alaska. USGS publications. Online at: <http://pubs.usgs.gov/pp/1769/>
- Prata, A. J., I. J. Barton, R. W. Johnson, K. Kamo, and J. Kingwell, 1991: Hazard from volcanic ash. *Nature*, **354**, 25.
- Rogers, A. B., Macfarlane, D. G. and Robertson, D. A. 2011: Complex Permittivity of Volcanic Rock and Ash at Millimeter Wave Frequencies. *IEEE Geosci. Remote Sen. Lett.* **8**(2), 298-302.
- Rose W.I., and Coauthors, 1995a: Ice in the 1994 Rabaul eruption cloud: Implications for volcano hazard and atmospheric effects. *Nature*, **375**, 477–479.

- Rose W.I., A. B. Kostinski, and L. Kelley, 1995b: Real-time C band radar observations of 1992 eruption clouds from Crater Peak, Mount Spurr volcano, Alaska. The 1992 eruptions of Crater Peak vent, Mount Spurr volcano, Alaska, *USGS Bull.* 2139, 19–26.
- Rose W.I., and Coauthors, 2013: The February-March eruption of Hekla, Iceland, from a satellite perspective. In: *Volcanoes and the earth atmosphere*. EDs: A. Robock and C. Oppenheimer, AGU Monographs. DOI: 10.1029/139GM07.
- Sawada, Y., 2004: Eruption cloud echo measured with C-band weather radar. [Available online at www.ofcm.noaa.gov/ICVAAS/Proceedings2004/pdf/entire-2ndICVAAS-Proceedings.pdf].
- Schneider, D.J., Scott, C., Wood, J., Hall, T., 2006, NEXRAD weather radar observations of the 2006 Augustine Volcanic eruption clouds: Eos (American Geophysical Union Transactions), v. 87, no. 52, Fall Meet. Supplement, abstract V51C-1686.
- Speirs, P.J., and D. A. Robertson, 2011: Measurement of airborne volcanic ash using millimeter-wave radars. *35th Conf. Radar Meteorol.*, Pittsburg, VA, 5A3. Available online at: <https://ams.confex.com/ams/35Radar/webprogram/Session25191.html>
- Textor C, H-F. Graf, M. Herzog, J.M. Oberhuber , W.I. Rose, G.G.J. Ernst, 2006a: Volcanic particles in explosive eruption columns. Part I: *J. Volcanol. Geotherm. Res.*, **150**, 359 – 377.
- Textor C, H-F. Graf, M. Herzog, J.M. Oberhuber , W.I. Rose, G.G.J. Ernst, 2006b: Hydrometeor-ash particle growth in volcanic eruption column. Part II: numerical experiments. *J. Volcanol. Geotherm. Res.* **150**, 378-394.
- Vidal L., S. Nesbitt, P. Salio, S. Osoro, C. Farias, A. Rodriguez, J. Serra, G. Caranti, 2015: C-band dual polarization observations of a massive volcanic eruption in South America. *37th Conf. Radar Meteorol.*, Norman, OK. Available online at: <https://ams.confex.com/ams/37RADAR/webprogram/Paper276312.html>
- Vulpiani, G., M. Montopoli, E. Picciotti, and F. S. Marzano, 2011: On the use of a polarimetric X-band weather radar for volcanic ash clouds monitoring. *35th Conf. Radar Meteorol.*, Norman, OK. Available online at: <https://ams.confex.com/ams/35Radar/webprogram/Session28568.html>
- Wardojo, E. 2015: The capability of a single polarization C-band radar to detect volcanic ash

(some cases of volcanic eruption in Indonesia). *37th Conf. Radar Meteorol.*, Norman, OK, 2015. Available online at:

<https://ams.confex.com/ams/37RADAR/webprogram/Paper277415.html>

Webley, P.W., D. Atkinson, R. L. Collins, K. Dean, J. Fochesatto, K. Sassen, C. F. Cahill, A. Prata, C. J. Flynn, and K. Mizutani, 2008: Predicting and Validating the Tracking of a Volcanic Ash Cloud during the 2006 Eruption of Mt. Augustine Volcano. *Bull. Amer Meteorol. Soc.* Nov, 1647-1657.

Zehner, C., Ed., 2010: Monitoring volcanic ash from space: ESA–EUMETSAT workshop on the 14 April to 23 May 2010 eruption at the Eyjafjoll volcano, south Iceland. ESA Publ. STM-280, 110 pp. Available online at

<http://esamultimedia.esa.int/multimedia/publications/STM-280>.